Seismic stratigraphic framework and depositional history for Cretaceous and Cenozoic contourite depositional systems of the Mozambique Channel, SW Indian Ocean

Antoine Thiéblemont, F. Javier Hernandez-Molina, Ponte Jean-Pierre, Cécile Robin, François Guillocheau, Carlo Cazzola, François Raisson

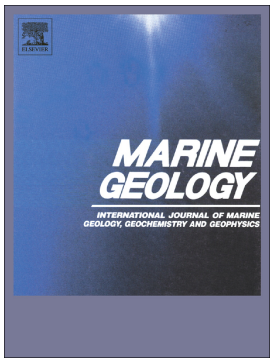

Seismic stratigraphic framework and depositional history for Cretaceous and Cenozoic contourite depositional systems of the Mozambique Channel, SW Indian Ocean

Antoine Thiéblemont, F. Javier Hernández-Molina, Ponte Jean-Pierre, Cécile Robin, François Guillocheau, Carlo Cazzola, François Raisson

PII: S0025-3227(20)30080-3

DOI: https://doi.org/10.1016/j.margeo.2020.106192

Reference: MARGO 106192

To appear in: *Marine Geology*

Received date: 27 August 2019

Revised date: 26 March 2020

Accepted date: 29 March 2020

Please cite this article as: A. Thiéblemont, F.J. Hernández-Molina, P. Jean-Pierre, et al., Seismic stratigraphic framework and depositional history for Cretaceous and Cenozoic contourite depositional systems of the Mozambique Channel, SW Indian Ocean, *Marine Geology* (2020), https://doi.org/10.1016/j.margeo.2020.106192

Seismic stratigraphic framework and depositional history for Cretaceous and Cenozoic contourite depositional systems of the Mozambique Channel, SW Indian Ocean

Antoine Thiéblemont[1, 2*], F. Javier Hernández-Molina[1], Ponte Jean-Pierre[3], Cécile Robin[3], François Guillocheau[3], Carlo Cazzola[4], François Raisson[2]

[1] Department of Earth Sciences, Royal Holloway, University of London, Egham, Surrey TW20 0EX, UK.

[2] TOTAL, R&D Frontier Exploration program, Avenue Larribau, 64000 Pau, France.

[3] Univ Rennes, CNRS, Géosciences Rennes - UMR 6118, 35000 Rennes, France

[4] TOTAL, Tour Coupole, 2 Pl. Jean Millier, 92078 Paris La Défense, France.

[*] Corresponding author. *E-mail address:* antoine.thieblemont@total.com

Abstract

This study describes previously unrecognized contourite depositional systems (CDSs) in the Mozambique Channel which constrain palaeoceanographic models for this area. The stratigraphic stacking patterns record nine seismic units (SU1 to SU9) separated by eight major discontinuities (a to h, oldest to youngest). Key seismic markers in CDS evolutionary history occur during Aptian-Albian (~122 Ma), late Cenomanian (94 Ma), early (38.2–36.2 Ma) and late (25–23 Ma) Oligocene, and early-middle Miocene (~17–15 Ma) epochs. These record onset (~122 to 94 Ma), growth (94 to 25–23 Ma), maintenance (25–23 to 17–15 Ma), and burial (17–15 Ma to the actual time) stages for CDSs. CDSs first develop during the onset stage which coincides with the opening and deepening of the African-Southern Ocean gateway (at 122 and 100 Ma, respectively). The growth stage, beginning in the late Cenomanian (94 Ma), correlates with the opening and deepening of the Equatorial Atlantic gateway. During the growth stage, two major shifts in sedimentary stacking pattern occur which coincide with

palaeoceanographic changes during the early (38.2–36.2 Ma) and late (25–23 Ma) Oligocene. These in turn coincide with the onset and local enhancement of Antarctic water masses. CDS growth continued until the early-middle Miocene during the maintenance stage (~17–15 Ma). Most CDS growth ceased at the end of the maintenance stage. Circulation of the North Atlantic water mass into the Southern Hemisphere led to a deepening of Antarctic water masses in the area.

Keywords: Seismic Stratigraphy, Morphology, Sedimentary Processes, Bottom Current, Cretaceous and Cenozoic, Mozambique Margin

1. Introduction

Deep marine sedimentary processes consist of pelagic particle settling through the water column, contour currents, and density currents (i.e., turbidity currents and mass-failures) (Rebesco et al., 2014, 2017). The first of these represents a background process that predominates only in abyssal areas. By contrast, density and contour currents affect many continental margins. Recent studies have demonstrated the importance of contour currents in shaping continental margins (Mosher et al., 2017) and have emphasized their role in deep-water sedimentation. Unlike episodic density currents, contour currents are relatively permanent and continuously affect other deep-water sedimentary processes (Rebesco et al., 2014). The interaction of contour currents with a continental margin can generate depositional features (contourites or contourite drifts), erosional features (moats, abraded surfaces, contourite channels, scours, and furrows), and depositional-erosional features (contourite terraces) (e.g., McCave and Tucholke, 1986; Rebesco and Stow, 2001; Viana et al., 2007; Hernández-Molina et al., 2009, 2017a, 2017b; García et al., 2009; Cattaneo et al., 2017). Moreover, recent studies have noted the relatively common interaction between episodic density currents and the more permanent contour currents in generating mixed features (e.g., Creaser et al., 2017; Sansom, 2018; Fonnesu et al., 2020).

When associated with a distinct water mass, these features form a contourite depositional system (CDS).

CDSs occur on most continental margins (e.g., Rebesco et al., 2014) and a single CDS may cover an area of 100,000 km^2 (Rebesco et al., 2017). As such they represent a major component of continental margin depositional environments. As previously observed by Hernández-Molina et al. (2009, 2010), major tectonic events can lead to large-scale palaeoceanographic shifts or climatic changes recorded by CDSs. As records of large-scale ocean dynamics, CDSs can inform palaeoceanographic interpretations. CDSs can also preserve and accumulate hydrocarbon deposits making them relevant to petroleum exploration (e.g., Viana et al., 2007).

The Mozambique Channel serves as a circulation gateway between the Indian Ocean and the Atlantic Ocean making it a significant location for decoding sedimentary and palaeoceanographic events (Castelino et al., 2015). Although Pleistocene to Quaternary palaeoceanographic records from this margin have been studied extensively (Hall et al., 2017 and references therein), the Early Cretaceous to Cenozoic history of both surface, intermediate, and deep-water circulation through the proto Indian - Atlantic Ocean gateway remains poorly understood. Significant gaps in understanding exist concerning surface to deep-water circulation around the continental margin and abyssal plain sedimentation.

Numerous CDSs have been identified within the Cenozoic stratigraphic record from the southern tip of Africa (south of 30°S latitude) (Niemi et al., 2000; Uenzelmann-Neben, 2001; Schlüter and Uenzelmann-Neben, 2007, 2008; Uenzelmann-Neben and Huhn, 2009; Uenzelmann-Neben et al., 2007, 2011; Gruetzner and Uenzelmann-Neben, 2015; Fisher and Unenzelman-Neben, 2018a, 2018b) and within Quaternary units of the Mozambican continental margin (north of 30°S latitude) (Flemming, 1978; Kolla et al., 1980; Wiles et al., 2014, 2017; Flemming and Kudrass, 2017; Breitzke et al., 2017; Miramontes et al., 2019a, 2019b; Thieblemont et al., 2019). Besides Preu et al.'s (2011) report on CDSs

within the stratigraphic record from the Mozambique Channel (north of 30°S latitude), no studies have addressed CDSs in this area. This gap limits understanding of their role in shaping the Mozambique Channel continental margin and abyssal plain from the Mesozoic to Cenozoic.

This research sought to improve understanding of Mozambican continental margin geological history through detailed examination of its Mesozoic to Cenozoic CDSs. A better understanding of this continental margin can constrain palaeoceanographic models of the southwest Indian Ocean.

2. Background and regional setting

2.1. Geological setting of the study area

The East African continental margin has a complex Mesozoic to Cenozoic tectonic and sedimentary history. The margin initially formed from the Mesozoic breakup of eastern (i.e., India, Antarctica, Australia, and Madagascar,) and western (i.e., South America and Africa) Gondwana, which occurred around 183–177 Ma (Eagles and König, 2008). Rifting of Gondwana transitioned into seafloor spreading during the Late Jurassic. This north-south oriented rift-to-drift phase created a marginal fracture ridge (i.e., DFZ, Davie Fracture Zone) (Coffin and Rabinowitz, 1987, 1992). The opening of the African-Southern Ocean gateway definitively separated these two landmasses, establishing the conditions for incipient intermediate and deep water exchange between the proto- Indian and Southern oceans, an event which represented the last phase in the process of rifting and subsequent sea floor spreading of the northern Mozambique basin (NMB) and southern Mozambique basin (SMB) between 159 Ma and 124 Ma (Jokat et al., 2003; König and Jokat, 2010; Leinweber and Jokat, 2012; Leinweber et al., 2013; Castelino et al., 2016).

The SMB (south of 25°S latitude) is now bounded to the west by the Mozambique ridge, about 100 km off the coast, and to the east by the Madagascar ridge (Sinha et al., 1981; Fischer et al., 2017) (**Fig. 1A**). The NMB (the study area for this work) lies between the DFZ and the Mozambican continental

margin at ~15°S to 25°S latitude. A continental basement high (i.e., Beira high) about 80 km off the coast of Mozambique (Mahanjane, 2012; Mueller et al., 2016) (**Fig. 1A**) bisects the NMB. The DFZ currently consists of a 1,200 km-long, N 170° trending topographic high connecting the east African margin and the southwest Madagascar margin through the Mozambique Channel. This structure is punctuated by seamounts (e.g., the Sakalaves seamount). The centre of the NMB also hosts several seamounts (Bassas Da India, Jaguar Bank, Europa, Hall Bank, Mt. Boucart) (**Fig. 1A**).

The NMB sedimentary record consists of two main sequences: (1) pre-breakup Karoo formation (i.e., Upper Carboniferous to the Lower Jurassic continental sediments and volcanic rocks), and (2) post-breakup Karoo formation (i.e., Upper Jurassic to Cenozoic continental transitional and marine sediments) (Nairn et al., 1991). The post-breakup Karoo succession reaches its maximum thickness along the shelf and upper slope in front of the Zambezi delta (>12 km of sedimentary accumulation since the Early Cretaceous; Salman and Abdula, 1995). Sediments are mainly sourced by the Zambezi river, which has a very large present-day catchment area (1,320,000 km^2) and sediment load of 20.10^6 to 48.10^6 t/yr (Milliman and Syvitski, 1992) (**Fig. 1A**). The catchment area evolved throughout three main deformation events that occurred since the Cretaceous: (1) uplift of the South African plateau in the Late Cretaceous (Moore, 1999), (2) uplift of the South African plateau from the Oligocene to early Miocene (Belton and Raab, 2010; Emmel et al., 2014), and (3) development and progressive southward migration of the East African Rift System (EARS) since the Oligocene (Chorowicz, 2005; Macgregor, 2015).

The EARS began to develop and propagate southwards beginning in the late Cenozoic (at ~30 Ma). It bifurcated into an eastern and western branch over the next 20 Myr until it finally propagated offshore along the NMB. Extensional deformation of the DFZ since the late Miocene records offshore evolution of the eastern branch while recent seismic activity around the NMB indicates that the western branch may be initiating offshore propagation (Mougenot et al., 1986; Franke et al., 2015) (**Fig. 1A**). Courgeon et al.

(2016) suggested that several seamounts (e.g., Hall Bank) drowned during the late Miocene-early Pliocene due to the influence of tectonic and volcanism correlating with the EARS.

2.2. The modern oceanographic setting

The southwest Indian Ocean is an area of active surface, intermediate, and deep-water circulation (**Fig. 1B** and A.1 in the supplementary material). The sedimentary processes in the southwest Indian Ocean are presently influenced by several water masses (e.g., Thiéblemont et al., 2019) whose understanding is an essential prerequisite to infer evolutionary scenarios of past ocean circulation. The main water masses contributing to the upper layers (<200 m water depth; wd) in the Mozambique Channel are the Tropical Surface Water (TSW) and the Subtropical Surface Water (STSW) (Wyrtki, 1973; Toole and Warren, 1993). The predominant water mass in the permanent thermocline of the Mozambique Channel (200–600 m wd) is the South Indian Central Water (SICW) (You, 1997). The TSW, STSW, and SICW enter the Mozambique Channel from the northern tip of Madagascar and feed into the Mozambique Current. Part of the STSW and the SICW enters the Mozambique Channel around the southern tip of Madagascar (Siedler et al., 2009) with the Southeast Madagascar Current. This component enters partly in the form of eddies (de Ruijter et al., 2004) and converges with the Mozambique Current (**Fig. 1B**). The Mozambique Current is characterized by large, southward-moving, mesoscale anticyclonic eddies with diameters >300 km (Schouten et al., 2002). These eddies can impose short-term circulation modulation over the entire depth and width of the channel (i.e., >2,500 m wd near 17°S latitude) (de Ruijter et al., 2002; Halo et al., 2014). The frequency of these events ranges from four to seven eddie passages per year (Schouten et al., 2003).

Intermediate waters in the Mozambique Channel are influenced by different water masses. The salty Red Sea Water (RSW) enters from the north at around 900–1,200 m wd (Donohue et al., 2000; Beal et al., 2000; Swart et al., 2010) while the fresh Antarctic Intermediate Water (AAIW) enters from the south

at around 800–1,500 m wd (Fine, 1993) (**Fig. 1B**). The Mozambique Undercurrent flows northward along the Mozambican slope carrying AAIW (Fine, 1993; de Ruijter et al., 2002), while mesoscale anticyclonic eddies transport RSW southward (Swart et al., 2010).

The deep-water masses of the Mozambique Channel consist of the North Atlantic Deep Water (NADW) at ~2,200–3,500 m wd and the Antarctic Bottom Water (AABW) flowing locally beneath it (below ~4,000 m wd). Toole and Warren (1993) showed that the DFZ in the Mozambique Channel effectively blocks the NADW from spreading north of ~15°S latitude (Mantyla and Reid, 1995; You, 1999). However, the influence of the NADW is seen up to about 2,000 m wd. The upper portion of the NADW thus passes over the sill at ~2,500 m depth while the remaining NADW flows along the eastern boundary of the NMB with a southerly returning current (van Aken et al., 2004; Ullgren et al., 2012) (**Fig. 1B**). The deepest part of the water column is occupied by the AABW. This water mass flows northward as a western boundary current along the SMB (Tucholke and Embley, 1984; Read and Pollard, 1999). Due to the shallowing of the basin to the north (>4,000 m wd), the AABW is deflected to form a southerly flowing boundary current along the east flank of the SMB (Kolla et al., 1980) (**Fig. 1B**).

3. Data and methods

3.1. Seismic reflection data

We analyzed two-dimensional (2D) multichannel seismic (MCS) reflection profiles collected by WesternGeco (**Fig. 2**). The seismic dataset was obtained during 2013/2014 geophysical cruises aboard the *Pacific Falcon* and *M/V WG Western Patriot* (**Table 1**). The primary dataset is a 36,179 km regional grid of linear 2D MCS reflection profiles, spaced at approximately 10 to 70 km intervals. The profiles were processed by 2D anisotropic Kirchhoff prestack time migration. Seismic data interpretation was performed using Sismage™ software. Discontinuities are expressed as reflections, with sequential “a” to “h” labels from older to younger. Nine seismic units (SU) were identified in this study, labeled “SU1” to

"SU9" from bottom to top. Discontinuities were mapped and gridded to produce continuous surfaces with a grid cell size of 40,000 m. Major physiographic domains (shelf, continental slope; hereafter "slope" for simplicity, continental rise; or simply "rise", and abyssal plain) were attributed to discontinuities a to h based on criteria defined by IHO and IOC (1983). Isochore maps were generated for all seismic units (i.e., SU1 to SU9). The thickness of units is reported in seconds or milliseconds two-way travel time (s or ms TWTT).

3.2. Geological age constraints

Discontinuities in 2D MCS reflection profiles were identified based on correlation with a previous study by Ponte et al. (2018). Chronostratigraphic interpretation referred to records from exploration wells X', X2, and X3 (Ponte et al., 2018) as well as abyssal plain scientific wells (DSDP Leg 25 Sites 248 and 249; Simpson et al., 1974a, 1974b; and DSDP Leg 26 Site 250; Davies et al., 1974) and information available from previous studies (Nairn et al., 1991; Salman and Abdula, 1995; Mahanjane, 2012; Castelino et al., 2015). **Figures 3** and A.2 in the supplementary material show a regional stratigraphic framework for the margin. These summarize results of shelf-to-abyssal plain regional stratigraphic correlation and list age constraints for seismic units and discontinuities.

The acoustic basement corresponds to the base of the post-breakup Karoo formation (i.e., >155 Ma; Nairn et al., 1991; Salman and Abdula, 1995). Above the Beira high, it correlates to the break-up unconformity described in Mahanjane (2012). Further offshore, this surface merges with what is interpreted to be the top of the oceanic basement based on marine magnetic anomalies (König and Jokat, 2010; Leinweber and Jokat, 2012; Leinweber et al., 2013; Mueller and Jokat, 2017) (**Fig. 3**). SU1 overlies the acoustic basement and is older than 129.4 Ma (i.e., Neocomian in age). SU2 developed between the upper Neocomian (129.4 Ma) and the Cenomanian-Turonian boundary (94 Ma). SU3 spans the Turonian to Senonian (94 to 67.3–63.2 Ma). SU4 formed during the Paleocene-Eocene interval

(67.3–63.2 to 38.2–36.2 Ma). SU5 formed during the Oligocene interval (38.2–36.2 Ma to 25–23 Ma). SU6 is dated from the early to middle Miocene (25–23 to 11.6 Ma). SU7 is dated late Miocene (11.6 Ma to 5.6 Ma) in age, SU8 is Pliocene (5.6 Ma to 2.8 Ma), and SU9 spans the base Pleistocene (2.8 Ma) to present day (Ponte et al., 2018) (**Fig. 3**).

3.3. Seismic facies units

Delineation of individual seismic facies units was based on continuity, amplitude, and configuration of seismic features as described in Sangree et al. (1978) and Sangree and Widmier (1979). Various seismic facies units were designated (**Fig. 4**) in terms of a depositional element. For density current features, we used the nomenclature developed in Mutti and Normark (1991). Their work differentiated turbidity currents as 1) channels and overbank, including levees and 2) sedimentary lobes. Mass-failures are hereafter termed mass transport deposits (MTDs) as defined by Shipp et al. (2011). Based on depositional elements, gross-depositional environment maps were generated for each seismic unit (SU1 to SU9).

3.4. Recognition of contourite depositional systems

The term contourites is used for "sediments deposited or substantially reworked by the persistent action of bottom currents" (Rebesco et al., 2014). Thick and extensive accumulations of sediments by bottom currents are defined as contourite drifts or drifts. Their identification is based on the following criteria defined by Rebesco (2005) and Rebesco et al. (2014): 1) external geometry, 2) bounding reflections, and 3) internal seismic facies (**Fig. 5**). Absent consensus on distinguishing large drifts from small ones, this study defined large drifts as those covering a plan view area of >1,000 km^2 (for a single drift) as defined in Campbell and Mosher (2015) along the Nova Scotia margin. We adopted the classification schemes for various types of drift morphology from McCave and Tucholke (1986), Faugères et al. (1999), Rebesco and Stow (2001), Rebesco (2005), and Rebesco et al. (2014).

Small contourite drifts formed from the interaction between contour currents and density currents (i.e., turbidity currents) are referred to as mixed drifts in Fonnesu et al. (2020). Creaser et al (2017) identified these features according to 1) asymmetry, 2) orientation, 3) dimensions, and 4) internal seismic facies (**Fig. 5**). In this study, a single mixed drift rarely exceeds 20 km in width and the entire observable down-dip length of the system is generally less than 40 km, suggesting that they are under 1,000 km^2 in plan view. However, this classification is not necessarily applicable in other areas (e.g., mixed drifts in Creaser et al., 2017 that are up to 40 km wide and over 50 km in down-dip direction).

Contour current erosional features are classified according to criteria given in Hernández-Molina et al. (2008) and García et al. (2009). These include: a) erosional surfaces, b) moats and contourite channels, and c) scours and furrows. Moats differ from contourite channels in terms of their genetic relationship with drifts. Criteria for recognition of erosional features include: 1) reflection truncation relationships, 2) association with sediment drifts (i.e., forming bounding surfaces in drift systems), and 3) inability to explain erosion by other processes, for example in deep basinal areas, far from the continental margin (**Fig. 5**).

4. Results

Seismic units and discontinuities were mapped to produce surface maps of the discontinuities a to h and isochore maps of seismic units 1 to 9 along the northern Mozambique basin (**Figs. 11** and **12**). **Figures 3** and A.2 (supplementary material) show seismic stratigraphic horizons mapped in this study. Initial mapping efforts confirmed the existence of contourite depositional systems (CDSs) first identified by Castelino et al. (2015). **Table 2** summarizes details concerning seismic facies of SU1 to SU9 and **figure 5** highlights the internal seismic facies of depositional, mixed and erosional features described below.

4.1. Large contourite drifts

Five large contourite drifts recognized in the study area were informally named based on their proximity to present-day oceanographic features. The oldest, large contourite drift, named the Beira drift, is located along a rise in the Middle Zambezi region, which occupies the northwestern edge of the Beira high (**Fig. 11**). The drift has a subtle mounded shape apparent in dip oriented seismic profiles (**Fig. 7**) and is slightly elongated in along a SSW-NNE direction (**Fig. 9**). The Beira drift reaches a maximum thickness of 1.8 s TWTT (**Fig. 12**). Stratigraphically, the drift developed within SU2, above regional seismic discontinuity a and below regional seismic discontinuity b (**Figs. 7** and **9**). The overall internal seismic facies of the drift consists of NNE prograding, high-continuity reflections with low acoustic response (**Fig. 5**).

Two others large contourite drifts, the Angoche and Zambezi drifts, occur along the slope of the Angoche region, and on the slope and rise in the Lower and Middle Zambezi regions, respectively (**Fig. 11**). The Angoche drift exhibits a plastered appearance and reaches a thickness of up to 2 s TWTT (**Fig. 12**). It thins landward and basinward according to dip-oriented seismic profiles (**Fig. 6**) but also laterally as documented in strike-oriented seismic profiles (**Fig. 9**). The drift is partially bisected by large downslope NNW-SSE oriented channels (**Fig. 9**). It occurs stratigraphically above the regional seismic discontinuity c and below the regional seismic discontinuity g (**Figs. 6** and **9**). The internal seismic facies of the Angoche drift consists mainly of aggrading parallel reflections with low acoustic response, which appear continuous during deposition of SU4 and SU5 and disrupted during deposition of SU6 and SU7 (**Fig. 5**).

The Zambezi drift has a mounded external geometry. It exhibits an elongated and separated appearance along the Lower Zambezi region and an elongated and detached appearance along the Middle Zambezi region (**Fig. 11**). In the Lower Zambezi region, the drift formed along a SW-NE trend, parallel to the distal limit of the slope (**Fig. 8**). In the Middle Zambezi region, the drift becomes detached along the rise with a pronounced arcuate geometry and an apparent steepened NE side relative to its

SW side. In this region, the drift attains a maximum thickness of ~2 s TWTT (**Figs. 7, 10A, 11** and **12**). The drift occurs stratigraphically above the regional seismic discontinuity c and below the regional seismic discontinuity f (**Figs. 7, 8** and **10A**). The internal seismic facies of the Zambezi drift consists mainly of aggrading, parallel high-continuity reflections with low acoustic response (**Fig. 5**). SU5 however contains reflections indicating drift crest migration to the SW (**Fig. 10A**).

The last two large contourite drifts, termed Limpopo drifts, are located on the abyssal pain, in the southerly part of the northern Mozambique basin. The drifts cover an area <1,000 km^2 but may be larger as they extend beyond the extent of study area (**Figs. 2** and **10B**). The northern Limpopo drift exhibits a mounded external geometry and reaches a maximum sedimentary thickness of ~1 s TWTT. It displays an elongated and detached appearance with a crest oriented WNW-ESE. The drift has a steep south side and a gently dipping, smooth north side (**Fig. 10B**). It occurs stratigraphically above regional seismic discontinuity b and below regional seismic discontinuity d. The drift exhibits mainly parallel, high-continuity reflections with low acoustic response (**Fig. 5**). Reflections within the drift show a predominantly aggradational stacking pattern, although northward drift crest migration is visible (**Fig. 10B**).

The second Limpopo drift is located further south. It occurs in the vicinity of a buried seamount. The drift is elongated in a SW-NE direction parallel to the trend of adjacent moats (*sensu* Rebseco et al., 2014) that flank the buried seamount. It reaches a maximum thickness of 1 s TWTT, which decreases in the vicinity of the moats (**Fig. 10B**). Stratigraphically, the drift develops above regional seismic discontinuity a, overlying a continuous, high to very high acoustic response reflector accompanied by occasional volcanic features (e.g., Polteau et al., 2008). It develops below regional seismic discontinuity d. The drift exhibits mainly parallel, high-continuity reflections with low acoustic response (**Fig. 5**).

4.2. Small contourite drifts (mixed drifts)

Mixed drifts are generally mounded in shape, and their elongation is almost perpendicular to the margin. They are defined by an irregular, erosional base, above which a channel develops. This channel is laterally accompanied by a unilateral levee and/or asymmetric levees (called “drift-levee” or “drift” in this case) that can reach more than 800 ms TWTT. The internal seismic facies of mixed drifts mostly consists of chaotic reflections with high acoustic response (the channel) laterally accompanied by downlapping, parallel, high-continuity to disrupted reflections with low acoustic response (the drift) (**Fig. 5**). Locally, these channels are filled by MTDs.

A mixed drift occurs along the slope and rise of the Middle Zambezi region. This drift runs parallel to a channel which propagates away from the slope in a predominantly NW-SE direction (**Figs. 9** and **13A**). Along the proximal part of the slope, the drift aggrades to the NE of the channel (**Fig. 13A**). Distally (i.e., lower slope to rise), the drift aggrades on both sides of the channel and becomes more symmetrical (**Fig. 9**). The mixed drift occurs stratigraphically above regional seismic discontinuity b and below regional seismic discontinuity c (**Fig. 9**).

More recent mixed drifts occur along the slope of the Middle Zambezi and Angoche regions. These run parallel to NW-SE oriented downslope channels (**Figs. 9** and **13B**) and aggrade to the NNE and NE of channels (**Figs. 9** and **13B**, respectively). Stratigraphically, they occur above the regional seismic discontinuity e and below regional seismic discontinuities g and f (**Figs. 9** and **13B**, respectively).

4.3. Sediment waves

Multiple wavy reflections with low-to-moderate acoustic response appear along the margin and are interpreted as sediment waves (e.g., Wynn and Stow, 2002) (**Fig. 5**). In some areas, sediment waves develop along the slope and rise (**Figs. 6, 8, 9** and **10A**). Sediment waves can make up almost the entire thickness of a drift or form only part of large drifts (**Figs. 7, 8** and **10A**). Wavelengths of sediment waves range from ~4–7 km, and wave heights can reach ~400 ms TWTT. Within the Zambezi drift, sediment

waves form much of SU5 between regional seismic discontinuities d and e. They occur along the drift's southwestern side in strike-oriented seismic profiles (**Fig. 10A**) and along its southeastern side on dip-oriented seismic profiles (**Figs. 7** and **8**). A large field of sediment waves appears along the rise of the Lower Zambezi region. These comprise of the succession between regional seismic discontinuities c and d which is here interpreted as SU4 (**Figs. 8** and **10A**). Wave crests strike north to south and apparent wave migration direction is to the west (Fig. A.3 in the supplementary material). A second large field of sediment waves occurs along the slope of the Angoche region during deposition of SU3 and above regional seismic discontinuity b (**Figs. 6** and **9**). Wave crests appear oriented along slope and exhibit apparent upslope wave migration. Horizontal data coverage for 2D multichannel seismic reflection profiles however was not adequate to map the detailed surface morphology and orientation of these features.

4.4. Erosional features

Erosional surfaces appear as high-continuity reflections with low to high acoustic response (**Fig. 5**). On the abyssal plain of the northern Mozambique basin, 2D multichannel seismic reflection profiles show erosion with the development of an erosional surface at regional seismic discontinuity b (i.e., top of SU2). The resultant erosional surface actively truncates underlying reflections to produce toplap terminations. In the rest of the study area, obstacles (e.g., in the vicinity of the buried seamount in **Fig. 10B**) appear to enhance erosion at discontinuity b. Along the abyssal plain, a prominent erosional surface (and hiatus) does not include SU5's deposits between regional seismic discontinuities d and e (**Figs. 3** and **10B**).

Moats and contourite channels are defined by an irregular concave base and originate by nondeposition and/or localized erosion. They are typically up to 5 km wide and can reach local depths of up to 500 ms TWTT. Contourite channels and moats appear as high-continuity reflections with low to

high acoustic response (**Fig. 5**). Along the abyssal plain, moats develop above regional seismic discontinuity a and below regional seismic discontinuity d, adjacent to the Limpopo drift and associated with a buried seamount (**Fig. 10B**). Moats are generally filled by high continuity, parallel to sub-parallel reflections with low to moderate acoustic response (**Figs. 5** and **10B**). Several channels have been identified at regional seismic discontinuity d forming during SU5 along the slope of the Lower Zambezi region. These channels are filled by fairly homogenous, high continuity, parallel to sub-parallel reflections with low to moderate acoustic response (**Figs. 5** and **8**). Although these channels may have been formed by density currents processes (i.e., turbidity currents), their apparent, along-slope trend suggests that they may record contour currents (therefore forming contourite channels). Additional 3D seismic datasets would be necessary to verify interpretations of these channels.

The most recent seismic units along the abyssal plain, SU6 through SU9, consist of successive large erosive depressions (>10 km in width) interpreted as scours (**Fig. 10B**). Their stratigraphic position immediately below similar, present-day seafloor features defined by Breitzke et al. (2017) supports this interpretation. Generally, scours appear as U-shaped continuous reflections with low to high acoustic response. They are filled by high continuity, parallel to sub-parallel reflections with low to moderate acoustic response, and locally by MTDs, which probably represent their collapsed flanks (**Figs. 5** and **10B**).

5. Discussion

5.1. Depositional patterns

Regional mapping has identified large Mesozoic to Cenozoic depocentres along the continental margin off Mozambique, where pre-existing structural elements strongly influenced deposition. Most of the depocentres occur northwest of the Beira high during the Mesozoic. Extensive contourite depositional systems (CDSs) determined whether depocentres accumulated beyond the Beira high

during the Cenozoic (**Fig. 12**). Different phases of deposition at different periods have been recognized along the basin. **Figure 14** presents series of depositional environment maps that summarize the main downslope and along-slope events that occurred during deposition of stratigraphic seismic units (SU) 1 to 9.

5.1.1. Seismic unit 1

SU1 deposits formed before the Neocomian (<129.4 Ma) and consist of heterogeneous density current deposits interspersed with hemipelagic sediments. Deep burial depths however make their exact identification difficult (**Figs. 6, 7, 8, 9** and **14**). SU1 mostly develops around the northwest bathymetric relief of the Beira high in the Lower Zambezi rise and along the slope and rise of the Middle Zambezi and Angoche regions (**Fig. 12**). Senkans et al. (2019) proposed that the basal part of SU1 in the Angoche region included an evaporitic or undercompacted shale layer (**Figs. 6** and **9**). This supports the interpretation of SU1 as a marine depositional environment. The salt layer may indicate a restricted marine environment. Absence of CDSs in the basin and an African-Southern Ocean gateway closed to oceanic circulation to the south (Castelino et al., 2016; **Fig. 16**) support this interpretation. Additional information could further resolve interpretations of SU1 depositional environments. In the abyssal plain, SU1 sediments occur primarily as hemipelagites overlying acoustic basement (**Fig. 10B**).

5.1.2. Seismic unit 2

Deposits between SU2's upper Neocomian (129.4 Ma) and the Cenomanian-Turonian boundary (94 Ma) mostly occur along the slope and rise of the Lower Zambezi region where they infill the depression formed around the northwest part of the Beira high (**Fig. 12**). These deposits are generally composed of sedimentary lobes interbedded with hemipelagic sediments with local MTDs (**Figs. 8** and **14**). The slope and rise of the Middle Zambezi region host, in lower parts of the unit, hemipelagites underlying the Beira drift. Sedimentary lobes cover these layers as does a MTD, which truncates its western flank (**Figs.**

7, 9 and **14**). In the Angoche region, sediments appear concentrated along the rise (**Fig. 12**). The lower part of the unit consists mostly of sedimentary lobes. The upper part of the unit hosts a MTD along the slope while hemipelagites dominate the rise (**Figs. 6** and **14**).

In the abyssal plain, SU2 includes initial CDSs developing as part of the Limpopo drift against the northern flank of a buried seamount. This unit occurs stratigraphically above a volcanic layer that could represent the Aptian-Albian volcanoclastic sediments drilled at DSDP Site 249 (Simpson et al., 1974b; Vallier, 1974). A widespread erosive discontinuity occurs at the top of SU2 along the abyssal plain. This feature likely formed due to enhanced bottom currents (e.g., Faugères et al., 1999) (**Fig. 10B**). As noted by other authors (e.g., Ludwig et al., 1968, Flores, 1973, Dingle et al., 1978, Martin et al., 1982, Dingle and Robson, 1985), this feature correlates with the hiatus (~25 Ma) expressed at the Mozambique ridge and Agulhas Plateau (e.g., Simpson et al., 1974b, Tucholke and Carpenter, 1977, Tucholke and Embley, 1984, Uenzelmann-Neben, 2002).

5.1.3. Seismic unit 3

SU3 encompasses the Turonian to Senonian (94 to 67.3–63.2 Ma) and records minor evidence of shelf progradation. It occurs only at smaller scales and is confined to the northwest part of the Beira high in the Lower Zambezi region (**Fig. 8**). The slope of the Lower Zambezi region includes sediment infill of the depression between the shelf and the submarine positive relief of the Beira high (**Fig. 12**). These deposits generally consist of sedimentary lobes interbedded with hemipelagic sediments (**Figs. 8** and **14**). The thick accumulation of sediments in the Zambezi region (**Fig. 12**) and its prograding shelf mark an increased sediment flux from the Zambezi river associated with rapid denudation of the uplifted South-African plateau during the Late Cretaceous (Walford et al., 2005; Ponte, 2018). In the Angoche region, deposits include a field of sediment waves that develops along the slope coevally with sedimentary lobes developing along the rise (**Figs. 6, 9** and **14**). The size of these sediment waves (e.g.,

Wynn and Stow, 2002) could suggest that contour currents contribute to their formation, but further analysis is necessary to fully constrain their origin. Along the slope and rise of the Middle Zambezi region, SU3 exhibits sedimentary lobes in its lower part while its upper part consists of a mixed drift. This suggests the combined influence of downslope and along-slope processes during SU3 deposition (**Figs. 7, 9** and **13A**). Interestingly, mixed drifts form in other areas of the southern hemisphere during the Late Cretaceous period (e.g., Uruguayan margin: Creaser et al., 2017; Argentine margin; Rodrigues et al., 2019). This could indicate the influence of well-developed bottom currents whose onset can be constrained as Late Cretaceous in age. Across the abyssal plain, the growth of the Limpopo drifts may support this hypothesis (**Fig. 10B**).

5.1.4. Seismic unit 4

Continental margin progradation diminishes during the Paleocene-Eocene interval represented by SU4 (67.3–63.2 to 38.2–36.2 Ma). In the Lower Zambezi and Middle Zambezi regions of the slope, the lower part of SU4 includes minor evidence of downslope processes (i.e., sedimentary lobes and channels) (**Figs. 8** and **14**). These give way to draping hemipelagites in the upper part of SU4, which are coeval to mound buildup with the development of carbonate platforms at the end of the Paleocene (Ponte et al., 2018). These deposits record major warming of the oceans and sea level rise at the end of the Paleocene (Haq et al., 1987; Zachos et al., 2001). Along the distal slope and rise of the Lower and Middle Zambezi regions, SU4 hosts the Zambezi drift and a large field of sediment waves (**Figs. 8, 10A, 14** and A.3 in the supplementary material). These sediment waves appear similar to those described along the abyssal plain of the Argentine basin, where they are interpreted to record weak and linear stratified bottom currents (e.g., Flood and Shor, 1988; Klaus and Ledbetter, 1988; Blumsack and Weatherly, 1989; Blumsack, 1993). The slope of the Angoche region is characterized by the growth of the Angoche drift which is incised by a downslope channel (**Figs. 6, 9** and **14**). Across the abyssal plain, SU4 records the growth of Limpopo drifts that develop similarly to those appearing in SU3 (**Fig. 10B**).

5.1.5. Seismic unit 5

Continental margin progradation (prograding clinoforms) occurs along the shelf of the Lower Zambezi and Middle Zambezi regions during the Oligocene as recorded in SU5 (38.2–36.2 Ma to 25–23 Ma) (**Fig. 8**). This unit marks the development of the modern Zambezi delta, a period of high sediment flux from the Zambezi river during uplift of the South-African plateau (Walford et al., 2005; Ponte, 2018; Ponte et al., 2018). The slope of the Lower and Middle Zambezi regions includes a late Eocene to Oligocene transition (reflector d) that hosts the development of large channels (**Fig. 8**). Although 2D multichannel seismic reflection profiles do not resolve whether or not these channels represent contourites, the early Oligocene marks the onset of significant deep-water circulation in the basin (Tucholke and Embley, 1984). Furthermore, homogenous and stratified seismic facies infilling SU5 channels could arise from winnowing and redistribution of sediments by bottom currents (e.g., Campbell and Mosher, 2015). The relative importance of this process remains uncertain however. Later in the Oligocene, downslope processes built lobes into SU5 around the Lower and Middle Zambezi regions (**Figs. 7, 8, 9** and **14**). The Zambezi drift hosts sediment waves developed along the distal limit of the slope and rise in the Zambezi region, where it determines the overall SU5 depositional pattern (**Figs. 7, 8, 10A, 12** and **14**). In the Angoche region, large channels and the Angoche drift develop along the slope (**Figs. 6, 9** and **14**). This pattern indicates a marked increase in sediment supply to the margin compared to that recorded by SU4 (Ponte, 2018). Along the southernmost part of the rise, SU5 exhibits sedimentary lobes potentially originating from the southernmost channels of the Lower Zambezi region or from channels further south of the study area (**Figs. 10A** and **14**). In the abyssal plain, SU5 is pre-empted by a strong erosional surface which coincides with a hiatus detected at DSDP Leg 25 Sites 248 and 249 (Simpson et al., 1974a, b) and DSDP Leg 26 Site 250 (Davies et al., 1974) (**Fig. 10B**).

5.1.6. Seismic unit 6

During deposition of the early to middle Miocene SU6 (25–23 to 11.6 Ma), clinoforms continue to prograde along the shelf of the Lower and Middle Zambezi regions (Ponte et al., 2018) (**Figs. 7** and **8**). Along the slope in the Lower Zambezi region, bathymetric relief of the Beira high deflects most channels to the north (**Fig. 14**). Sedimentary lobes ponded along the slope and rise of the Middle Zambezi and Angoche regions interfinger around the latter region with the evolving Angoche drift and associated incision channels (**Figs. 6, 7** and **9**). Some of these channels represent mixed drifts (**Fig. 9** and **Fig. 13B**) indicating continued influence of bottom currents. The bathymetric relief of the Zambezi drift confines sedimentary lobes to the south (i.e., Lower Zambezi rise) by acting as a "natural dam" (**Figs. 7, 10A** and **14**). Most sediments along the rise of the Lower Zambezi region categorize as hemipelagites but the lower part of SU6 forms part of the overall Zambezi drift (**Fig. 10A**). In the southernmost part of the rise and abyssal plain, reflection data show sedimentary lobes in SU6 bound to the south by bathymetric relief of the northern Limpopo drift (**Fig. 10B**). These relations indicate that gravity flow processes operate in this part of the margin during SU6 development and may associate with channels along the slope, south of the Beira high and the area covered in **Figure 14**. Sedimentary lobes develop during a period of coarse-grained (1–3 mm on average) sand deposition at Site 248 interpreted as a strong and rapid terrigenous influx along the African margin beginning in the middle Miocene (Simpson et al., 1974a). South of the northern Limpopo drift, SU6 to SU9 sediments are undifferentiated and host many erosional features (e.g., scours) which indicate vigorous bottom currents (**Fig. 10B**).

5.1.7. Seismic unit 7, 8, and 9

Although a distinct period of drift development occurs in the late Miocene SU7 (11.6 Ma to 5.6 Ma), it marks the transition from primarily along-slope processes back to downslope gravity flow processes, as well as during the latter Pliocene SU8 (5.6 Ma to 2.8 Ma) and SU9 (Pleistocene or 2.9 Ma to present) (**Fig. 14**). This transition mostly reflects an increase in sediment supply to the margin from the late Miocene to the Pleistocene (Walford et al., 2005). Along the shelf of the Lower Zambezi and Middle

Zambezi regions, prograding clinoforms extend 80 km (Ponte et al., 2018) (**Figs. 7** and **8**). These formed coevally with extensive channels and MTDs along the slope (**Figs. 7, 8, 9** and **14**). The MTDs provide indirect evidence of slope instability resulting from rapid delivery of sediment to the slope. Sediments may pass over the Beira high which relieves flow in channels otherwise constricted by sediments funneled into preexisting bypass routes along basement features. Reorganization of channels along the slope enabled deposition of sedimentary lobes along the rise in the Lower Zambezi region (**Figs. 8, 10A** and **14**). In the Middle Zambezi region, these channels converge downslope to join the modern Zambezi Valley (**Fig. 14**). Data from DSDP Site 250 document a major influx of detrital material at the beginning of the Pliocene (Davies et al., 1974) which forms a large sedimentary lobe (Droz and Mougenot, 1987; Fierens et al., 2019). This feature and its position confirm transfer of sediments towards the abyssal plain through this pathway.

5.2. Insights into Mesozoic and Cenozoic circulation in the Mozambique Channel

The development and burial of contourite depositional systems recorded by these stratigraphic units accompanied significant changes in ocean circulation and coincided with major tectonic events such as the opening and closing of oceanic gateways (Rebesco et al., 2014). The palaeobathymetric model of Castelino et al. (2016) provides a useful framework for understanding ocean circulation on geological time scales. This framework consists of intermediate waters (<4,000 m wd) and deep waters (>4,000 m wd) which correspond to the slope and rise area and to the abyssal plain, respectively. The study area experienced four main (informal) stages of ocean circulation: onset, growth (sub-divided into sub-stages 1 - 3), maintenance, and burial.

5.2.1. The onset stage

Onset of intermediate circulation occurs with the development of the Beira drift. Onset of this drift is poorly constrained but occurs above regional seismic discontinuity a (i.e., >129.4 Ma) suggesting onset

of oceanic circulation in the Early Cretaceous (Aptian–Albian). Castelino et al. (2015) report observations suggesting Late Cretaceous onset (**Fig. 15**). The former interpretation agrees with findings of Uenzelmann-Neben et al. (2017), which infer oceanic circulation through the African-Southern Ocean (A-SO) gateway beginning in Albian time (~110 Ma). Onset of deep circulation occurs with the development of the southern Limpopo drift at the Albian-Cenomanian boundary (~100.5 Ma) and records initiation of a deep-water connection through the A-SO gateway (~100 Ma, Lawver et al., 1992; König and Jokat, 2006) (**Figs. 15** and **16**).

5.2.2. The growth stage

The growth stage divides into three sub-stages. Sub-stage 1 occurs during deposition of SU3 (Late Cretaceous), sub-stage 2 during SU4 (Paleocene-Eocene), and sub-stage 3 during SU5 (Oligocene).

At intermediate water depths, the sub-stage 1 records burial of the Beira drift, where density current features associated with uplift of the South African plateau probably mask effects of bottom currents on sediment (Ponte et al., 2018) (**Fig. 15**). The mixed drift represents the only preserved evidence of bottom currents. These document the influence of a northeast flowing, intermediate current interpreted by Voigt et al. (2013) and Donnadieu et al. (2016) to weaken in distal areas where more symmetric drift levees bound the channel. Along the abyssal plain, the erosional surface referred to as discontinuity b marks the onset of sub-stage 1. This indicates bottom currents operating around the Cenomanian to Turonian transition. Fisher and Uenzelmann-Neben (2018a) linked this intensive circulation to the Turonian (~91 Ma) onset of a long-lasting cooling trend after the Cretaceous thermal maximum. Opening and deepening of the Equatorial Atlantic Gateway may have caused this event (Poulsen et al., 2001, 2003; Huber et al., 2002; Murphy and Thomas, 2012; Friedrich et al., 2012). Limpopo drifts developed above this erosional surface in response to circulation components of

northward deep currents that might be associated to the southern component water (Robinson et al., 2010) (**Figs. 15** and **16**).

During sub-stage 2, partial cessation of density currents favors development of contour current features. Large contourites appear in the basin, including the Zambezi and Angoche drifts. A large field of sediment waves indicates intensification and expansion of intermediate currents in distal areas. This intensification may indicate greater overall circulation with cooler conditions during the early to late Eocene (Zachos et al., 2001) (**Fig. 15**). Sediment wave orientation suggests predominantly northeastward-flowing bottom currents. Numerical simulations by Uenzelmann-Neben et al. (2017) and ε_{Nd} signatures reported for Eocene sediments by Thomas et al. (2003) also indicate northward flow in the study area. Deep circulation remained similar to that operating during sub-stage 1 and development of the southern Limpopo drifts (**Figs. 15** and **16**).

Erosional features (i.e., contourite channels) formed during sub-stage 3 could mark the onset of more vigorous bottom currents at intermediate water depths. The emergence of these currents may reflect major Oligocene palaeoceanographic changes in the Southern Ocean associated with the opening of the Drake Passage (Zachos et al., 2001; Potter and Szatmari, 2009) (**Fig. 15**). These enabled full development of the Antarctic Circumpolar Current (ACC) around the Eocene/Oligocene boundary (31 Ma: Lawver and Gahagan, 2003; 34 Ma: Barker and Thomas, 2004; ~33 Ma: Livermore et al., 2004). The expansion of the East Antarctic ice sheet (Barrett, 1996) and a new thermohaline circulation pattern contributed to initiation of Circumpolar Deep Water (CDW) and a proto-Antarctic Bottom Water (AABW) (Kennett, 1982; Niemi et al., 2000; Hernández-Molina et al., 2009; Lindeque et al., 2016; Uenzelmann-Neben et al., 2017) (**Fig. 16**). During this interval, the Zambezi and Angoche drifts experienced significant vertical accumulation. The absence of SU5 deposits in abyssal environments appears consistent with interpretations given in Leclaire (1974) that infer an erosional zone resulting from strong western-boundary undercurrents supplied by AABW. These presumably operated by late Oligocene to early

Miocene times. The unconformity developed along the margins of the Cape Basin, Agulhas Plateau, and Mozambique Basin off South Africa marks the principal pathways of abyssal flow for AABW through the region (Tucholke and Embley, 1984) (**Figs. 15** and **16**).

5.2.3. The maintenance stage

The maintenance stage develops during SU6 deposition. Despite the general downslope depositional setting proposed for SU6, the Zambezi and Angoche drifts experienced growth during this stage. This could be linked to rising sea level associated with warmer conditions from the end of the Oligocene (27–26 Ma) until the middle Miocene (~15 Ma) (Haq et al., 1987; Zachos et al., 2001). We therefore propose similar oceanographic conditions in the early Miocene rather than in the Oligocene. This interpretation, consistent with that of Heezen and Hollister (1971), holds that the AABW forms a huge loop in the northern part of the Mozambique basin (**Figs. 15** and **16**).

5.2.4. The burial stage

Termination of the Zambezi drift growth marked the onset of major palaeoceanographic changes at basin scales with cooling after the Mid-Miocene Climatic Optimum (17–15 Ma). Palaeoceanographic changes correspond to an increase in deep-water circulation (AABW) in the Southern Hemisphere (Kennett, 1982; Uenzelmann-Neben et al., 2017). This coincided with Miocene glaciation, sea-level fall (Zachos et al., 2001), the expansion of the eastern Antarctic ice sheet (Mercer, 1983; Pierce et al., 2017), and initiation of North Atlantic Deep Water (NADW) circulation in the Southern Hemisphere (Kennett, 1982) (**Fig. 15**). This last change may have generated a deepening of the AABW, resulting in a NADW/AABW interface at depths of ~3,500–4,000 m wd. These processes buried the Zambezi drift. Along the slope, the upper boundary of the NADW is probably interfaced with the newly formed Antarctic Intermediate Water (AAIW) (**Fig. 16**). The onset of AAIW may be the result of changes that took place during the middle Miocene, coeval with the initiation of the permanent eastern Antarctic ice-

sheet (Mercer, 1983) (**Fig. 15**). Under the influence of NADW, the Zambezi drift ceased to be active due to burial but the Angoche drift now under the influence of the AAIW remained active during SU7 deposition. Downslope processes predominate in this area however.

5.3. Conceptual model for the evolution of large contourite drifts

Hydrodynamic processes behind small contourite drifts (i.e., mixed turbidite-contourite drifts) have been recently studied by several authors (e.g., Miramontes et al., 2020), mostly as potential high-value hydrocarbon reservoirs (Fonnesu et al., 2020; Fuhrmann et al., 2020). However, the hydrodynamic processes at the origin of large elongated-mounded and sheeted contourite drifts identified in many abyssal plains and continental margins are still underexplored despite, for example, their potential as seal-rocks or their role as topographic barriers or conduits for subsequent gravity flow deposits (e.g., Viana et al., 2007). In the Mozambique Channel, several large elongated-mounded contourite drifts have been recognized with the available 2D multichannel seismic reflection profile dataset (i.e., Limpopo drifts, Zambezi drift, Angoche drift, and Beira drift). However, the use of 3D seismic volumes is required to provide a detailed geometrical analysis of these large contourite drifts. Despite of that, this study unravels the role of large contourite drifts in the formation of ponded systems (e.g., sedimentary lobes) and the influence of downslope channels pathways, modifying the sedimentary stacking pattern at the basin scale. Therefore, hydrodynamic processes behind their formation should be addressed and could be applied more globally. Here, we attempt to characterize the formation of the Zambezi drift, which represents an important component in the sedimentary and palaeoceanographic evolution of the Mozambique basin.

In the Lower Zambezi region, the Zambezi drift is characterized by an erosional channel (~10 km wide) in its landward and upslope area (**Figs. 8** and **17A**). It might be similar to a downslope channel coevally with the Zambezi drift's formation (i.e., for the time of deposition of SU4, SU5, and SU6) (**Fig.**

14), but deviated in an SW-NE trend by the remnant positive relief of the Beira High. Here, because the asymmetry of the Zambezi drift and its association with the channel, it might be confused with an asymmetric channel–levee complex (e.g., Migeon et al., 2006). But, the fact that there is not any large feeder gravitational system connected to this channel, its parallel distribution to the paleo-slope, and its association to an adjacent elongated-mounded and separated drift allows to interpret this channel as a contourite moat (e.g., McCave and Tucholke, 1986; Faugères et al., 1999; Rebesco and Stow, 2001; Masson et al., 2002). It results from the increased flow path of the proto- Antarctic Bottom Water (AABW) due to the Coriolis effect directing the current core against the adjacent slope (**Fig. 17A**), eroding the left side and depositing sediment on the right side where the current velocity is lower, as proposed by Faugères et al. (1999). Along the western continental slopes in the southern hemisphere, moats occur on the left sides of elongated-mounded and separated drifts confined by the slope physiography, suggesting north-eastward-directed main flow on this margin (e.g., Llave et al., 2001). However, we do not exclude the possibility that some smaller downslope channels connect to this moat, contributing locally for the drift's development (e.g., overspill of fine-grained sediments) and the infill of the moat (e.g., filled by coarser-grained sediments) (**Figs. 14** and **17**). Furthermore, sediment waves within the drift may develop by contour currents but are similar, in form and dimensions, to waves formed by turbidity currents (**Figs. 8** and **17A**) (e.g., Wynn and Stow, 2002). Therefore, further studies should emphasize about criteria to distinguish waves formed by these contrasting mechanisms in the study area.

In the Middle Zambezi region, the previous elongated-mounded and separated drift becomes detached to the slope and resembles other giant mounded drifts described in the Transkei basin by Niemi et al. (2000) or in the Argentine basin by Hernández-Molina et al. (2010). These drifts are built in open deep marine settings (i.e., in which the core current migration is not confined by the slope physiography). In these systems, drifts are distinguished by their asymmetric mounded external shapes

with erosion on the steep sides and continuous deposition onto the gentler sides, which are typically partly covered with sediment waves, and the drift's crest migration is leftward down current (in the Southern Hemisphere). In the Mozambique Channel, the Zambezi drift in the Middle Zambezi region represents a sedimentary system characterized in its early development phase by a prominent crest, a steep and more erosive SW side, and a smooth gently dipping and depositional NE side (**Fig. 17B**). The drift's crest migration is towards the NE suggesting that the proto- AABW flow path is towards the SE with the main core of the water mass located in the southwest part of the drift (**Fig. 17B**). However, in the late phase of the drift's development the system changes completely with deposition focused on the SW side of the drift where large sediment waves develop, and erosion and/or non-deposition dominate the NW side of the drift (**Fig. 17C**). We interpret the shift between early and late phases by a change in the position of the main core of the water mass, now located in the northeast part of the drift (**Fig. 17C**). The most likely scenario for the upslope migrating sediment waves on its SW flank is that these waves create by weak contour currents between 0.1–0.3 m/s, based on the criteria from Stow et al. (2009).

We consider the changes in the drift's development during the late phase to occur during a late Oligocene period (26–23 Ma). At this time, Pekar et al. (2006) suggest a reduction and a weakening of the proto- AABW in comparison to the early Oligocene period (34–26 Ma). The configuration of the basin with 1) a northward shallowing of the seafloor (Castelino et al., 2016), 2) the inherit morphology of the Zambezi drift initial phase, and 3) a deeper proto- AABW top interface controls the change in the position of the proto- AABW main core. We suggest that the drift moves from an open-marine system to a "slope-confined" system in which the main core of the current moves on the left side of the elongated-mounded drift (in the Southern Hemisphere), confined by the slope physiography (**Fig. 17C**). This scenario of a late Oligocene proto- AABW current condition may have been true for the early Miocene SU6 (Pekar et al., 2006), consistent with the drift's maintenance stage (**Fig. 17C**).

An important point concerned the various sediment inputs for the construction of this drift: sediments could be of pelagic-hemipelagic origin, turbidity currents origin from adjacent slopes, and bottom currents origin with local erosion and longer-distance transport (**Fig. 17**). Sediment deposition can be enhanced as well by external factors such as topographic effects, distal input from terrestrial sources, local erosion around obstacles, etc. (Hernández-Molina et al., 2006; Stow et al., 2008). Moreover, regional sediment distribution could be increased due to the effect of internal waves associated with the CDW / AABW interface and its interaction with the continental slope, inducing sediment resuspension and transport through nepheloid layers (e.g., Bourgault et al., 2014) (**Fig. 17**). This confirms the multi-processes interaction for the drift's formation and the necessity to integrate oceanographic and sedimentological studies for a better understanding of these giant contourite drifts.

Conclusion

Based on observations of the study area, interpretations are summarized as three main conclusions:

- Large contourite drifts developed from Albian-Aptian times with optimal conditions during the Oligocene. Small mixed contourite drifts developed locally during interaction between density currents and contour currents in the Late Cretaceous and early-middle Miocene. These established a paleo-bottom current direction. All bottom current evidence suggests predominantly south to north circulation along the African margin during the Mesozoic and Cenozoic. Significant erosional phases caused by bottom currents have been identified from sediments deposited during the Turonian and late Oligocene. The timing of these erosional phases appears to be similar with that observed for other areas of the African margin.
- The main phases of CDS growth and burial coincide with major tectonic changes, which strongly influence the paleoceanography of the margin. The sedimentary record thus confirms the

connection between global events and CDS development to demonstrate that these features represent important records for underexplored margins of the Southern Hemisphere.

- This approach could be extended with further study of the African continental margin. The paucity of deep-sea wells and the sparse coverage of multichannel 2D seismic reflection profiles represent a major gap in records of palaeoceanographic circulation in this area (i.e., different water masses and their respective water depths, and criteria for palaeo-bottom current directions). Detailed analysis of three-dimensional seismic reflection data along with high-resolution stratigraphic data from other deep-water sites can help constrain understanding of the margin and its relation to global events.

Acknowledgments

The Authors sincerely thank INP and WesternGeco for use the study area seismic dataset. This research formed part of the Ph.D. thesis for A. Thiéblemont funded by TOTAL as part of the Frontier Exploration research program. The research was conducted in the scope of "The Drifters" Research Group of the Royal Holloway University of London (UK), and is related to projects CTM 2012-39599-C03, CGL2016-80445-R, and CTM2016-75129-C3-1-R. We acknowledge the suggestions of Marco Fonnesu and three anonymous referees that helped in improving this work.

Tables

Table 1. Seismic survey parameters for the dataset interpreted this study.

Survey name/ area:	*2D Mozambique/ Mozambique*
Acquired by:	*WesternGeco*
Survey type:	*2D Marine streamer*
Vessel:	*Pacific Falcon, M/V WG Western Patriot*
Recording dates:	*Apr 2013-Jan 2014*
Sail line prefix:	*MBWG13*
Coverage	*460,000 km2, 36,179 km of 2D lines*

Source	*1 array* *24 airguns TUNED BOLT* *(83.33 l)*
Marine streamer	*10,300.0 m*
Shot interval	*25 m*
Sampling rate	*2 ms*
Recorder	*Triacq V*
Recording length	*12,288 ms*
Processing Software	*WesternGeco's Omega™ Software*
Processing sequence	*2D anisotropic Kirchhoff PSTM* *Time migration*

Table 2. Seismic facies for seismic units (SU9 to SU1) along the shelf, slope, rise, and abyssal plain of the Mozambique margin. Legend for seismic configuration: 1a = prograding clinoforms; 2a = disrupted; 3a = parallel/subparallel (Type 1); 3b = parallel/subparallel (Type 2); 4a = hummocky; 5a = chaotic (Type 1); 5b = chaotic (Type 2). See **Fig. 4** for the type of seismic configuration.

Units	Age	Seismic facies				Thickness and distribution
		Boundaries	Top/ bottom termination	Seismic configuration	External shape	
SU9	Actual time 2.8 Ma	Seafloor Reflector h	Truncation; concordant configuration Onlap; concordant configuration	1a, 2a, 3a, 3b, 4a, 5a and 5b	Wedge, sheet and lens	Maximum thickness in the shelf of the Lower Zambezi region (>700 ms TWTT); increase its thickness in the rise of the Lower Zambezi region (>400 ms TWTT)
SU8	2.8 Ma 5.6 Ma	Reflector h Reflector g	Truncation; concordant configuration Onlap; concordant configuration			
SU7	5.6 Ma 11.6 Ma	Reflector g Reflector f	Truncation; concordant configuration Onlap; concordant configuration			
SU6	11.6 Ma 25-23 Ma	Reflector f Reflector e	Truncation; concordant configuration Concordant configuration; onlap	1a, 2a, 3a, 3b, 4a and 5b	Wedge, lens, mound and sheet	Major thickness in the shelf of the Lower Zambezi region (900 ms TWTT); important in the slope and rise of the Middle Zambezi and Angoche regions (>700 ms TWTT)
SU5	25-23 Ma 38.2-36.2	Reflector e Reflector d	Concordant configuration; truncation Concordant configuration;	1a, 2a, 3a, 3b, 4a and 5b	Sheet, wedge and mound	Major thickness in the shelf of the Lower Zambezi region (500 ms TWTT) ; important in the slope and rise of the Middle Zambezi (>1000 ms TWTT)

	Ma		onlap			
SU4	38.2-36.2 Ma 67.3-63.2 Ma	Reflector d Reflector c	Truncation; concordant configuration Concordant configuration; onlap	2a, 3a, 3b, and 5b	Sheet and mound	No significant thickness. Major thickness in the slope and rise of the Middle Zambezi region (>400 ms TWTT)
SU3	67.3-63.2 Ma 94 Ma	Reflector c Reflector b	Concordant configuration; truncation Concordant configuration; onlap	1a, 2a, 3a, 3b, 4a, 5a and 5b	Wedge, sheet and mound	Important in the slope and rise of the Middle Zambezi region (1.5 s TWTT)
SU2	94 Ma 129.4 Ma	Reflector b Reflector a	Concordant configuration; truncation Concordant configuration; onlap	2a, 3a, 3b, 4a and 5a	Wedge, sheet and mound	Maximum thickness against the NW flank of the Beira high in the slope and rise of the Lower and Middle Zambezi regions (1.8 s TWTT)
SU1	129.4 Ma >129.4 Ma	Reflector a Acoustic basement	Concordant configuration; truncation Concordant configuration; onlap	2a, 3a, 3b and 5a	Wedge and sheet	Major thickness in the rise of the Angoche and Middle Zambezi regions (>1.1 s TWTT)

Figures captions

Figure 1. A) Regional and geological setting of the Mozambican continental margin. Filled yellow circles represent DSDP Leg 25 Sites 242, 243, 244, 248, and 249 (Simpson et al., 1974a, b), IODP 361 Sites U1474, U1476, U1477, and U1478 (Hall et al., 2017), and DSDP Leg 26 Site 250 (Davies et al., 1974). White thick line represents the present-day Zambezi river catchment. Dashed blue-white lines represent major fault zones (thick) also reported by Chorowicz (2005) and Macgregor (2015). Thin dashed blue-white lines represent inferred fault zones. Red circles represent earthquakes since 1960 (M>4; USGS). Dashed black line represents the location of the Beira High. Legend: DFZ = Davie Fracture Zone, ZV = Zambezi Valley, NMB = Northern Mozambique Basin, SMB = Southern Mozambique Basin, MozR = Mozambique Ridge, MdgR = Madagascar Ridge. Bathymetric map from Weatherall et al. (2015). B) General sketch showing the main circulation paths along the Mozambique Channel. Map also shows the shelf circulation (based on Malauene et al., 2018). Legend: ZV = Zambezi Valley, DFZ = Davie Fracture Zone, NMB = Northern Mozambique Basin, SMB = Southern Mozambique Basin, MC = Mozambique Current, me = Mesoscale Eddy, e = Eddy, SEMC =

Southeast Madagascar Current. Dashed black line represents the location of the Beira High. Bathymetric map from Weatherall et al. (2015). Figure A.1 of the supplementary material gives a more complete sketch. Black box represents the location of the study area in **Fig. 2**.

Figure 2. Location of seismic profiles (multichannel seismic reflection profiles; MSC) along the Mozambique Channel as well as exploration wells X', X2, and X3 (Ponte et al., 2018), DSDP Leg 25 Sites 243 and 244 (Simpson et al., 1974a, b), and IODP 361 Site U1477 (Hall et al., 2017). Legend for oceanographic features: ZV = Zambezi Valley; DFZ = Davie Fracture Zone; NMB = Northern Mozambique Basin.

Figure 3. Regional stratigraphic sketch showing correlations with exploration wells X2 and X3 (Ponte et al., 2018). It shows the main physiographic domains, stratigraphic discontinuities, and seismic units identified by this research. Figure A.2 in the supplementary material gives more complete sketch.

Figure 4. Description and examples of seismic facies spanning the shelf, slope, rise, and abyssal plain of the Mozambique margin for seismic units (SU9 to SU1). Depths given in ms TWTT.

Figure 5. Seismic facies template for a contourite depositional system. White and black arrows represent boundaries terminations. Depths given in ms TWTT.

Figure 6. Seismic profile for the Angoche region of the Mozambique margin and its interpretation. Profile location shown in **Fig. 2**. Inset showing sediment waves in SU3. Seismic profile courtesy of INP and WesternGeco.

Figure 7. Seismic profile for the Middle Zambezi region of the Mozambique margin and its interpretation. Profile location shown in **Fig. 2**. Inset showing a mixed drift in SU3. Seismic profile courtesy of INP and WesternGeco.

Figure 8. Seismic profile for the Lower Zambezi region of the Mozambique margin and its interpretation. Profile location in **Fig. 2**. Inset showing channels in SU5. Seismic profile courtesy of INP and WesternGeco.

Figure 9. Seismic profile for the Lower and Middle Zambezi regions parallel to the Mozambique margin with interpretation. Profile location shown in **Fig. 2**. Inset-1 showing a mixed drift in SU3. Inset-2 showing a mixed drift in SU6 and SU7. Seismic profile courtesy of INP and WesternGeco.

Figure 10. A) Seismic profile for the Lower Zambezi region of the Mozambique margin with interpretation. Profile location shown in **Fig. 4**. Inset showing sediment waves in SU5 within the Zambezi drift. B) Seismic profile along the abyssal plain of the Mozambique margin with interpretation. Profile location shown in **Fig. 4**. Isopach map covers the abyssal plain of SU4 (in ms TWTT) and highlights the location of the Limpopo drifts (dashed red line) along with the inferred current direction. Seismic profiles courtesy of INP and WesternGeco.

Figure 11. Surface maps (in ms TWTT) for the main discontinuities (reflectors a to h), showing the main physiographic domains (shelf, slope, and rise) of the margin at the time of deposition. Location of the Beira high is given by a dashed black line. Main drifts (Beira, Angoche, and Zambezi) shown for the time of deposition before the discontinuity (dashed red lines). Solid white lines represent physiographic boundaries between the shelf, slope, and the rise.

Figure 12. Isochore maps (in ms TWTT) of the Mozambique margin for SU1 through SU9 showing the location of the Beira high (dashed black line). Main drifts (Beira, Angoche, and Zambezi) for the time of deposition are indicated (dashed red lines). Solid white lines represent physiographic boundaries between the shelf, slope, and rise.

Figure 13. Examples of mixed drifts from the study area. A) Mixed drift in SU3 along the continental slope of the Middle Zambezi region. B) Another example of a SU6 mixed drift on the continental

slope of the Middle Zambezi region. Profile locations shown in **Fig. 14**. C) Block diagram (adapted from Fonnesu et al., 2020) of the interaction between NE directed contour currents and perpendicular, downslope (SE) flowing density currents. Seismic profiles courtesy of INP and WesternGeco.

Figure 14. Gross depositional environment maps showing the main depositional elements for SU1 through SU9. Beira high limit is represented by a dashed black line.

Figure 15. Chart of major Cretaceous to Cenozoic global events (tectonic, climatic, sea level, and palaeoceanographic events) (Zachos et al., 2001; Hernández-Molina et al., 2017b). These global changes are correlated with the regional stratigraphy of the Mozambique Margin. Geological time scale from Ogg et al. (2016). Global sea level records: (1) from 0 to 7 Ma (in purple) (Miller et al., 2005), (2) from 7 to 100 Ma (in black and light blue) (Miller et al., 2005), (3) from 100 to 140 Ma (in light gray) (Sahagian et al., 1996), (4) from 7 to 100 Ma (in black and red) (Kominz et al., 2008), (5) deep-sea benthic foraminiferal oxygen (in red) and carbon (in green) isotopic curves (Cramer et al., 2009). Light yellow: basin accumulation rates for whole Zambezi sedimentary system (in km^3/Ma) from Ponte (2018). Abbreviations in alphabetic order: AABW = Antarctic Bottom Water, ACC = Antarctic Circumpolar Current, A-SO = Atlantic-Southern Ocean, CAS = Central American Seaway, EAIS = Eastern Antarctic Ice Sheet, EARS = Eastern Africa Rift System, ETM2 = Eocene Thermal Maximum 2, K-T = Cretaceous/ Tertiary, MME = Mid-Maastrichtian Event, MTD = Mass-Transport Deposit, NADW = North Atlantic Deep Water, PETM (ETM1) = Paleocene/Eocene Thermal Maximum (Eocene Thermal Maximum 1), S-A = Southern Africa, SCW = Southern Component Water, WAIS = Western Antarctic ice Sheet.

Figure 16. Palaeoceanographic evolution of the Mozambique Channel based on this study and on Fischer and Uenzelmann-Neben, (2018a) (and references therein). Palaeobathymetric

reconstructions based on Castelino et al. (2016). Time frames cover A) 130 Ma, B) 120 Ma, C) 100 Ma, D) 75 Ma, E) 40 Ma, F) 30 Ma, G) 15 Ma, H) 10 Ma. Light grey represents areas not included in their palaeobathymetric reconstruction. A - SO gateway closed to circulation is represented by a thick dashed red line. Abbreviations for water-masses: (proto-) AABW = Antarctic Bottom Water, AAIW = Antarctic Intermediate Water, CDW = Circumpolar Deep Water, NADW = North Atlantic Deep Water. Legend for oceanographic features: NMB = Northern Mozambique Basin, SMB = Southern Mozambique Basin, MozR = Mozambique Ridge, A - SO = African Southern Ocean gateway, NV = Natal Valley, APa = Agulhas Passage, AP = Agulhas Plateau, MdgR = Madagascar Ridge.

Figure 17. Conceptual 3D sketch for the construction of the Zambezi drift. A) Seismic section of the Zambezi drift for the Lower Zambezi region. B) Seismic section of the Zambezi drift for the Middle Zambezi region during its early phase of construction (34–26 Ma). Sketch showing the theoretical bottom shear stress values (in $N.m^{-2}$) along the seafloor. Note that the critical shear stress for resuspension of muddy silts is proposed in the range of 0.03–0.1 $N.m^{-2}$ for deep-sea environments (e.g., McCave and Swift, 1976). C) Seismic section of the Zambezi drift for the Middle Zambezi region during its late phase of construction (26–23 Ma) with theoretical bottom shear stress values (in $N.m^{-2}$) along the seafloor. Abbreviations: proto-AABW = proto-Antarctic Bottom Water, CDW = Circumpolar Deep Water. Seismic profiles courtesy of INP and WesternGeco.

References

Barker, P.F., Thomas, E., 2004. Origin, signature and palaeoclimatic influence of the Antarctic Circumpolar Current. Earth Science Reviews. Vol 66, Issues 1-2, 143-162. http://dx.doi.org/10.1016/j.earscirev.2003.10.003

Barrett, P.J., 1996. Antarctic paleoenvirornment through Cenozoic times – a review. Terra Antarctica. Vol 3, Issue 2, 103-119.

Beal, L.M., Chereskin, T.K., Lenn, Y.D., Elipot, S., 2006. The sources and mixing characteristics of the Agulhas Current. Journal of Physical Oceanography. Vol 36, Issue 11, 2060-2074. http://dx.doi.org/10.1175/JPO2964.1

Beal, L.M., Ffield, A., Gordon, A.L., 2000. Spreading of Red Sea overflow waters in the Indian Ocean. Journal of Geophysical Research: Oceans. Vol 105, Issue C4, 8549-8564. http://dx.doi.org/10.1029/1999JC900306

Belton, D.X., Raab, M.J., 2010. Cretaceous reactivation and intensified erosion in the Archean-Proterozoic Limpopo Belt, demonstrated by apatite fission track thermochronology. Tectonophysics. Vol 480, Issue 1, 99-108. http://dx.doi.org/10.1016/j.tecto.2009.09.018

Blumsack, S.L., 1993. A model for the growth of mudwaves in the presence of time-varying currents. Deep-Sea Research II. Vol 40, 4/5, 963-974. http://dx.doi.org/10.1016/0967-0645(93)90043-M

Blumsack, S.L., Weatherly, G.L., 1989. Observations of the nearby flow and a model for the growth of mudwaves. Deep-Sea Research. Vol 36, 9, 1327-1339. http://dx.doi.org/10.1016/0198-0149(89)90086-1

Bourgault, D., Morsilli, M., Richards, C., Neumeier, U., Kelley, D.E., 2014. Sediment resuspension and nepheloid layers induced by long internal solitary waves shoaling orthogonally on uniform slopes. Continental Shelf Research. Vol 72, 21-33. http://dx.doi.org/10.1016/j.csr.2013.10.019

Breitzke, M., Wiles, E., Krocker, R., Watkeys, M.K., Jokat, W., 2017. Seafloor morphology in the Mozambique Channel: evidence for long-term persistent bottom-current flow and deep-reaching eddy activity. Marine Geophysical Research. Vol 38, Issue 3, 241-269. http://dx.doi.org/10.1007/s11001-017-9322-7

Campbell, D.C., Mosher, D.C., 2015. Geophysical evidence for widespread Cenozoic bottom current activity from the continental margin of Nova Scotia, Canada. Marine Geology. http://dx.doi.org/10.1016/j.margeo.2015.10.005

Castelino, J., Reichert, C., Klingelhoefer, F., Aslanian, D., Jokat, W., 2015. Mesozoic and Early Cenozoic sediment influx and geomorphology of the Mozambique Basin. Marine and Petroleum Geology. Vol 66, Part 4, 890-905. http://dx.doi.org/10.1016/j.marpetgeo.2015.07.028

Castelino, J.A., Eagles, G., Jokat, W., 2016. Anomalous bathymetry and paleobathymetry models of the Mozambique Basin and Riiser Larsen Sea. Earth and Planetary Science Letters. Vol 455, 25-37. http://dx.doi.org/10.1016/j.epsl.2016.09.018

Cattaneo, A., Miramontes, E., Samalens, K., Garreau, P., Caillaud, M., Marsset, B., Corradi, N., Migeon, S., 2017. Contourite identification along Italian margins: The case of the Portofino drift (Ligurian Sea). Marine and Petroleum Geology. Vol 87, 137-147. http://dx.doi.org/10.1016/j-marpetgeo.2017.03.026

Chorowicz, J., 2005. The east African rift system. Journal of African Earth Sciences. Vol 43, Issue 1-3, 379-410. http://dx.doi.org/10.1016/j.jafrearsci.2005.07.019

Coffin, M. F., Rabinowitz, P. D., 1992. The Mesozoic East African and Madagascan conjugate continental margins; stratigraphy and tectonics. In: Watkins, J.S., Zhigiang, F., McMillen, K.J. (Eds.), Geology and Geophysics of Continental Margins. AAPG. Vol 53, 207-240. http://dx.doi.org/10.1306/M53552C12

Coffin, M.F., Rabinowitz, P.D., 1987. Reconstruction of Madagascar and Africa: Evidence from the Davie Fracture Zone and Western Somali Basin. Journal of Geophysical Research. Vol 92, Issue B9, 9385-9406. http://dx.doi.org/10.1029/JB092iB09p09385

Courgeon, S., Jorry, S.J., Camoin, G.F., BouDagher-Fadel, M.K., Jouet, G., Révillon, S., Bachèlery, P., Pelleter, E., Borgomano, J., Poli, E., Droxler, A.W., 2016. Growth and demise of Cenozoic isolated carbonate platforms: New insights from the Mozambique Channel seamounts (SW Indian Ocean). Marine Geology. Vol 380, 90-105. http://dx.doi.org/10.1016/j.margeo.2016.07.006

Cramer, B.S., Toggweiler, J.R., Wright, J.D., Katz, M.E., Miller, K.G., 2009. Ocean overturning since the late Cretaceous: inferences from a new benthic foraminiferal isotope compilation. Paleoceanography. Vol 24, Issue 4, 1-14. http://dx.doi.org/10.1029/2008PA001683

Creaser, A., Hernández-Molina, F.J., Badalini, G., Thompson, P., Walker, R., Soto, M., Conti, B., 2017. A Late Cretaceous mixed (turbidite-contourite) system along the Uruguayan Margin: Sedimentary and palaeoceanographic implications. Marine Geology. Vol 390, 234-253. http://dx.doi.org/10.1016/j.margeo.2017.07.004

Davies, T.A., Luyendyk, B.P., Rodolfo, K.S., Kempe, D.R.C., McKelvey, B.C., Leidy, R.D., Horvath, G.J., Hyndman, R.D., Thierstein, H.R., Herb, R.C., Boltovskoy, E., Doyle, P., 1974. Site 250. In: Davies, T.A., Luyendyk, B.P., Rodolfo, K.S., Kempe, D.R.C., McKelvey, B.C., Leidy, R.D., Horvath, G.J., Hyndman, R.D., Thierstein, H.R., Herb, R.C., Boltovskoy, E., Doyle, P. (Eds.), Initial Reports of the Deep Sea Drilling Project. Washington (U.S. Government Printing Office). Vol 25, 21-73. http://dx.doi.org/10.2973/dsdp.proc.26.103.1974

de Ruijter, W.P.M., Ridderinkhof, H., Lutjeharms, J.R.E., Schouten, M.W., Veth, C., 2002. Observations of the flow in the Mozambique Channel. Geophysical Research Letters. Vol 29, Issue 10, 1502. http://dx.doi.org/10.1029/2001GL013714

de Ruijter, W.P.M., van Aken, H.M., Beier, E.J., Lutjeharms, J.R.E., Matano, R.P., Schouten, M.W., 2004. Eddies and dipoles around south Madagascar: formation, pathways and large-scale impact. Deep Sea Research Part I: Oceanographic Research Papers. Vol 51, Issue 3, 383-400. http://dx.doi.org/10.1016/j.dsr.2003.10.011

Dingle, R.V., Goodlad, S.W., Martin, A.K., 1978. Bathymetry and stratigraphy of the northern Natal Valley (SW Indian Ocean): a preliminary account. Marine Geology. Vol 28, Issues 1-2, 89-106. http://dx.doi.org/10.1016/0025-3227(78)90099-3

Dingle, R.V., Robson, S., 1985. Slumps, canyons and related features on the continental margin off East London, SE Africa (SW Indian Ocean). Marine Geology. Vol 67, Issues 1-2, 37-54. http://dx.doi.org/10.1016/0025-3227(85)90147-1

Donnadieu, Y., Puceat, E., Moiroud, M., Guillocheau, F., Deconinck, J.-F., 2016. A better-ventilated ocean triggered by Late Cretaceous changes in continental configuration. Nature Communications 7, 10316. http://dx.doi.org/10.1038/ncomms10316

Donohue, K.A., Beal, L.M., Firing, E., 2000. Comparison of three velocity sections of the Agulhas Current and Agulhas Undercurrent. Journal of Geophysical Research: Oceans. Vol 105, Issue C12, 28,585-28,593. http://dx.doi.org/10.1029/1999JC000201

Droz, L., Mougenot, D., 1987. Mozambique upper fan: origin of depositional units. AAPG Bulletin. Vol 71, Issue 11, 1355-1365.

Eagles, G., König, M., 2008. A model of plate kinematics in Gondwana breakup. Geophysical Journal International. Vol 173, Issue 2, 703-717. http://dx.doi.org/10.1111/j.1365-246X.2008.03753.x

Emmel, B., Kumar, R., Jacobs, J., Ueda, K., Van Zuilen, M., Matola, R., 2014. The low-temperature thermochronological record of sedimentary rocks from the central Rovuma Basin (N Mozambique) – Constraints on provenance and thermal history. Gondwana Research. Vol 25, 1216-1229. http://dx.doi.org/10.1016/j.gr.2013.05.008

Faugères, J.-C., Stow, D.A.V., Imbert, P., Viana, A.R., 1999. Seismic features diagnostic of contourite drifts. Marine Geology. Vol 162, 1-38. http://dx.doi.org/10.1016/S0025-3227(99)00068-7

Fierens, R., Droz, L., Toucanne, S., Raisson, F., Jouet, G., Babonneau, N., Miramontes, E., Landurain, S., Jorry, S., 2019. Late Quaternary geomorphology and sedimentary processes in the Zambezi turbidite system (Mozambique Channel). Geomorphology. Vol 334, 1-28. https://doi.org/10.1016/j.geomorph.2019.02.033

Fine, R.A., 1993. Circulation of Antarctic Intermediate Water in the South Indian Ocean. Deep-Sea Research Part 1: Oceanographic Research Papers. Vol 40, Issue 10, 2021-2042. http://dx.doi.org/10.1016/0967-0637(93)90043-3

Fischer, M. D., Uenzelmann-Neben, G., 2018b. Neogene modifications of circulation in the northeastern African-Southern Ocean gateway. Geochemistry, Geophysics, Geosystems. Vol 19, Issue 12, 4673-4693. http://dx.doi.org/10.1029/2018GC007644

Fischer, M.D., Uenzelmann-Neben, G., 2018a. Late Cretaceous onset of current controlled sedimentation in the African-Southern Ocean gateway. Marine Geology. Vol 395, 380-396. http://dx.doi.org/10.1016/j.margeo.2017.11.017

Fischer, M.D., Uenzelmann-Neben, G., Jacques, G., Werner, R., 2017. The Mozambique Ridge: a document of massive multistage magmatism. Geophysical Journal International. Vol 208, Issue 1, 449-467. http://dx.doi.org/10.1093/gji/ggw403

Flemming, B.W., 1978. Underwater sand dunes along the southeast African continental margin-observations and implications. Marine Geology. Vol 26, Issue 3-4, 177-198. http://dx.doi.org/10.1016/0025-3227(78)90059-2

Flemming, B.W., Kudrass, H-F., 2017. Large dunes on the outer shelf off the Zambezi Delta, Mozambique: evidence for the existence of a Mozambique Current. Geo-Marine Letters. Vol 38, Issue 1, 95-106. http://dx.doi.org/10.1007/s00367-017-0515-5

Flood, R.D., Shor, A., 1988. Mud waves in the argentine basin and their relationship to regional bottom circulation patterns. Deep-Sea Research. Vol 35, 943-971. http://dx.doi.org/10.1016/0198-0149(88)90070-2

Flores, G., 1973. The Cretaceous and Tertiary sedimentary basins of Mozambique and Zululand. In: Blant, G. (Eds.), Sedimentary Basins of the African Coast. Part 2, South and East Coast. Association of African Geological Surveys, Paris, 81-111.

Fonnesu, M., Palermo, D., Galbiati, M., Marchesini, M., Bonamini, E., Bendias, D., 2020. A new world-class deep-water play-type, deposited by the syndepositional interaction of turbidity flows and bottom currents: The giant Eocene Coral Field in northern Mozambique. Marine and Petroleum Geology. Vol 11, 179-201. http://dx.doi.org/10.1016/j.marpetgeo.2019.07.047

Franke, D., Jokat, W., Ladage, S., Stollhofen, H., Klimke, J., Lutz, R., Mahanjane, E.S., Ehrhardt, A., Schreckenberger, B., 2015. The offshore East African Rift System: Structural framework at the toe of a juvenile rift. Tectonics. Vol 34, Issue 10, 2086-2104. http://dx.doi.org/10.1002/2015TC003922

Friedrich, O., Norris, R.D., Erbacher, J., 2012. Evolution of middle to Late Cretaceous oceans - a 55 m.y. record of Earth's temperature and carbon cycle. Geology. Vol 40, Issue 2, 107-110. http://dx.doi.org/10.1130/G32701.1

Fuhrmann, A., Kane, I.A., Clare, M.A., Ferguson, R.A., Schomacker, E., Bonamini, E., Contreras, F.A., 2020. Hybrid turbidite-drift channel complexes: An integrated multiscale model. Geology. https://doi.org/10.1130/G47179.1

García, M., Hernández-Molina, F.J., Llave, E., Stow, D.A.V., León, R., Fernández-Puga, M.C., Díaz del Río, V., Somoz, L., 2009. Contourite erosive features caused by the Mediterranean Outflow Water in the Gulf of Cadiz: Quaternary tectonic and oceanographic implications. Marine Geology. Vol 257, Issue 1-4, 24-40. http://dx.doi.org/10.1016/j.margeo.2008.10.009

Gruetzner, J., Uenzelmann-neben, G., 2015. Contourite drifts as indicators of Cenozoic bottom water intensity in the eastern Agulhas Ridge area, South Atlantic. Marine Geology. Vol 378, 350-360. http://dx.doi.org/10.1016/j.margeo.2015.12.003

Hall, I.R., Hemming, S.R., LeVay, L.J., Barker, S., Berke, M.A., Brentegani, L., Caley, T., Cartagena-Sierra, A., Charles, C.D., Coenen, J.J., Crespin, J.G., Franzese, A.M., Gruetzner, J., Han, X., Hines, S.K.V., Jimenez Espejo, F.J., Just, J., Koutsodendris, A., Kubota, K., Lathika, N., Norris, R.D., Periera dos Santos, T., Robinson, R., Rolinson, J.M., Simon, M.H., Tangunan, D., van der Lubbe, J.J.L., Yamane, M., and Zhang, H., 2017. Expedition 361 summary, in: Hall, I.R., Hemming, S.R., LeVay, L.J., and the Expedition 361 Scientists, South African Climates (Agulhas LGM Density Profile). Proceedings of the International Ocean Discovery Program, 361: College Station, TX (International Ocean Discovery Program). http://dx.doi.org/10.14379/iodp.proc.361.101.2017

Halo, I., Backeberg, B., Penven, P., Ansorge, I., Reason, C., Ullgren, J.E., 2014. Eddy properties in the Mozambique Channel: A comparison between observations and two numerical ocean circulation models. Deep Sea Research Part II: Topical Studies in Oceanography. Vol 100, 38-53. http://dx.doi.org/10.1016/j.dsr2.2013.10.015

Haq, B.U., Hardenbol, J., and Vail, P.R., 1987, Chronology of fluctuating sea levels since the Triassic. Science. Vol 235, 1156-1167. http://dx.doi.org/10.1126/science.235.4793.1156

Heezen, B. C., Hollister, C.D., 1971. The face of the deep. Oxford University Press, 659 pp.

Hernández-Molina, F.J., Campbell, S., Badalini, G., Thompson, P., Walker, R., Soto, M., Conti, B., Preu, B., Thieblemont, A., Hyslop, L., Miramontes, E., Morales, E., 2017a. Large bedforms on contourite terraces: Sedimentary and conceptual implications. Geology. Vol 46, 27-30. http://dx.doi.org/10.1130/G39655.1

Hernández-Molina, F.J., Larter, R.D., Maldonado, A., 2017b. Neogene to Quaternary stratigraphic evolution of the Antarctic Peninsula, Pacific Margin offshore of Adelaide Island: Transitions from a non-glacial, through glacially-influenced to a fully glacial state. Global and Planetary Change. Vol 156, 80-111. http://dx.doi.org/10.1016/j.gloplacha.2017.07.002

Hernández-Molina, F.J., Llave, E., Stow, D.A.V., 2008. Continental slope contourites. In: Rebesco, M., Camerlenghi, A. (Eds.), Contourites Developments in Sedimentology. Elsevier, Vol 60, pp. 379-408.

Hernández-Molina, F.J., Llave, E., Stow, D.A.V., García, M., Somoza, L., Vázquez, J.T., Lobo, F., Maestro, A., Díaz del Río, V., León, R., Medialdea, T., Gardner, J., 2006. The contourite depositional system of the Gulf of Cadiz: a sedimentary model related to the bottom current activity of the Mediterranean outflow water and the continental margin characteristics. Deep Sea Research Part II: Topical Studies in Oceanography, 53, 11-13, 1420-1463. http://dx.doi.org/10.1016/j.dsr2.2006.04.016

Hernández-Molina, F.J., Paterlini, M., Somoza, L., Violante, R., Arecco, M.A., de Isasi, M., Rebesco, M., Uenzelmann-Neben, G., Neben, S., Marshall, P., 2010. Giant mounded drifts in the Argentine Continental Margin: origins, and global implications for the history of thermohaline circulation. Marine and Petroleum Geology. Vol 27, Issue 7, 1508-1530. http://dx.doi.org/10.1016/j.marpetgeo.2010.04.003

Hernández-Molina, F.J., Paterlini, M., Violante, R., Marshall, P., de Isasi, M., Somoza, L., Rebesco, M., 2009. Contourite depositional system on the Argentine slope: an exceptional record of the influence of Antarctic water masses. Geology. Vol 37, Issue 6, 507-510. http://dx.doi.org/10.1130/G25578A.1

Huber, B.T., Norris, R.D., MacLeod, K.G., 2002. Deep-sea paleotemperature record of extreme warmth during the Cretaceous. Geology. Vol 30, 123-126. http://dx.doi.org/10.1130/0091-7613(2002)030<0123:DSPROE>2.0.CO;2

IHO and IOC, 1983. Standardization of Undersea Feature Names: Guidelines, Proposal Form, Terminology. International Hydrographic Bureau, Monaco, pp. 27.

Jokat, W., Boebel, T., König, M., Meyer, U., 2003. Timing and geometry of early Gondwana breakup. Journal of Geophysical Research. Vol 108, Issue B9. http://dx.doi.org/10.1029/2002JB001802

Kennett, J.P., 1982. Marine Geology. Prentice Hall, 813 pp.

Klaus, A., Ledbetter, M.T., 1988. Deep-sea sedimentary processes in the Argentine Basin revealed by high-resolution seismic records (3.5 kHz echograms). Deep-sea Research. Vol 35, 899-917. http://dx.doi.org/10.1016/0198-0149(88)90067-2

Kolla, V., Eittreim, S., Sullivan, L., Kostecki, J.A., Burckle, L.H., 1980. Current-controlled, abyssal microtopography and sedimentation in Mozambique Basin, Southwest Indian Ocean. Marine Geology. Vol 34, Issue 3-4, 171-206. http://dx.doi.org/10.1016/0025-3227(80)90071-7

Kominz, M.A., Browning, J.V., Miller, K.G., Sugarman, P.J., Mizintseva, S., Scotese, C.R., 2008. Late Cretaceous to Miocene sea-level estimates from the New Jersey and Delaware coastal plain coreholes: an error analysis. Basin Research. Vol 20, Issue 2, 211-226. http://dx.doi.org/10.1111/j.1365-2117.2008.00354.x

König, M., Jokat, W., 2006. The Mesozoic breakup of the Weddell Sea. JGR Solid Earth. Vol 111, Issue B12. http://dx.doi.org/10.1029/2005JB004035

König, M., Jokat, W., 2010. Advanced insights into magmatism and volcanism of the Mozambique Ridge and Mozambique Basin in the view of new potential field data. Geophysical Journal International. Vol 180, Issue 1, 158-180. http://dx.doi.org/10.1111/j.1365-246X.2009.04433.x

Lawver, L.A., Gahagan, L.M., 2003. Evolution of Cenozoic seaways in the circum-Antarctic region. Palaeogeography, Palaeoclimatology, Palaeoecology. Vol 198, Issues 1-2, 11-37. http://dx.doi.org/10.1016/S0031-0182(03)00392-4

Lawver, L.A., Gahagan, L.M., Coffin, M.F., 1992. The development of Paleoseaways around Antarctica. The Antarctic Paleoenvironment: a perspective on global change: part one. Vol 56. http://dx.doi.org/10.1029/AR056p0007

Leclaire, L., 1974. 20. Late Cretaceous and Cenozoic Pelagic Deposits - Paleoenvironment and Paleooceanography of the Central Western Indian Ocean. In: Davies, T.A., Luyendyk, B.P., Rodolfo, K.S., Kempe, D.R.C., McKelvey, B.C., Leidy, R.D., Horvath, G.J., Hyndman, R.D., Thierstein, H.R., Herb, R.C., Boltovskoy, E., Doyle, P. (Eds.), Initial Reports of the Deep Sea Drilling Project. Washington (U.S. Government Printing Office). Vol 25, 481-513. http://dx.doi.org/10.2973/dsdp.proc.25.120.1974

Leinweber, V.T., Jokat, W., 2012. The Jurassic history of the Africa-Antarctica Corridor - new constraints from magnetic data on the conjugate continental margins. Tectonophysics. Vol 530-531, 87-101. http://dx.doi.org/10.1016/j.tecto.2011.11.008

Leinweber, V.T., Klingelhoefer, F., Neben, S., Reichert, C., Aslanian, D., Matias, L., Heyde, I., Schreckenberger, B., Jokat, W., 2013. The crustal structure of the Central Mozambique continental margin d Wide-angle seismic, gravity and magnetic study in the Mozambique Channel, Eastern Africa. Tectonophysics. Vol 599, 170-196. http://dx.doi.org/10.1016/j.tecto.2013.04.015

Lindeque, A., Gohl, K., Henrys, S., Wobbe, F., Davy, B., 2016. Seismic stratigraphy along the Amundsen Sea to Ross Sea continental rise: a cross-regional record of pre-glacial to glacial processes of the West Antarctic margin. Palaeogeography, Palaeoclimatology, Palaeoecology. Vol 443, 183-202. http://dx.doi.org/10.1016/j.palaeo.2015.11.017

Livermore, R., Eagles, G., Morris, P., Maldonado, A., 2004. Shackleton fracture zone: no barrier to early circumpolar ocean circulation. Geology. Vol 32, 9, 797-800. http://dx.doi.org/10.1130/G20537.1

Llave, E., Hernández-Molina, F.J., Somoza, L., Díaz del Río, V., Stow, DAV., Maestro, A., Alveirinho Dias, J.M., 2001. Seismic stacking pattern of the Faro-Albufeira contourite system (Gulf of Cadiz): a Quaternary record of paleoceanographic and tectonic influences. Marine Geophysical Research, 22, 5-6, 487-508. http://dx.doi.org/10.1023/A:1016355801344

Ludwig, W.J., Nafe, J.E., Simpson, E.S.W., Sacks, S., 1968. Seismic-refraction measurements on the Southeast African continental margin. Journal of Geophysical Research. Vol 73, Issue 12, 3707-3719. http://dx.doi.org/10.1029/JB073i012p03707

Macgregor, D., 2015. History of the development of the East African Rift System: a series of interpreted maps through time. Journal of African Earth Sciences. Vol 101, 232-252. http://dx.doi.org/10.1016/j.jafrearsci.2014.09.016

Mahanjane, E.S., 2012. A geotectonic history of the northern Mozambique Basin including the Beira High e a contribution for the understanding of its development. Marine and Petroleum Geology. Vol 36, Issue 1, 1-12. http://dx.doi.org/10.1016/j.marpetgeo.2012.05.007

Malauene, B.S., Moloney, C.L., Lett, C., Roberts, M.J., Marsac, F., Penven, P., 2018. Impact of offshore eddies on shelf circulation and river plumes of the Sofala Bank, Mozambique Channel. Journal of Marine Systems. Vol 185, 1-12. http://dx.doi.org/10.1016/j.jmarsys.2018.05.001

Mantyla, A.W., Reid, J.L., 1995. On the origins of deep and bottom waters in the Indian Ocean. Journal of Geophysical Research: Oceans. Vol 100, Issue C2, 2417-2439. http://dx.doi.org/10.1029/94JC02564

Martin, A.K., Goodlad, S.W., Salmon, D.A., 1982. Sedimentary basin in-fill in the northernmost Natal Valley, hiatus development and Agulhas Current palaeo-oceanography. Journal of the Geological Society. Vol 139, 183-201. http://dx.doi.org/10.1144/gsjgs.139.2.0183

Masson, D.G., Howe, J.A., Stoker, M.S., 2002. Bottom-current sediment waves, sediment drifts and contourites in the northern Rockall Trough. Marine Geology, Vol 192, Issues 1-3, 215-237. https://doi.org/10.1016/S0025-3227(02)00556-X

McCave, I. N., Kiefer, T., Thornalley, D. J. R., Elderfield, H., 2005. Deep flow in the Madagascar-Mascarene Basin over the last 150,000 years. Philosophical Transactions of the Royal Society A. Vol 363, 81-99. http://dx.doi.org/10.1098/rsta.2004.1480

McCave, I.N., Swift, S.A., 1976. A physical model for the rate of deposition of fine-grained sediments in the deep sea. GSA Bulletin. Vol 87, Issue 4, 541-546. http://dx.doi.org/10.1130/0016-7606(1976)87<541:APMFTR>2.0.CO;2

McCave, I.N., Tucholke, B.E., 1986. Deep current controlled sedimentation in the western North Atlantic. In: Vogt, P.R., Tucholke, B.E. (Eds.), The Western North Atlantic Region. Geology of North America. Vol M, 451-468. http://dx.doi.org/10.1130/DNAG-GNA-M.451

Mercer, J.H., 1983. Cenozoic glaciation in the southern hemisphere. Annual Review of Earth and Planetary Science. Vol 11, 99-132. http://dx.doi.org/10.1146/annurev.ea.11.050183.000531

Migeon, S., Mulder, T., Savoye, B., Sage, F., 2006. The Var turbidite system (Ligurian Sea, northwestern Mediterranean)—morphology, sediment supply, construction of turbidite levee and sediment waves: implications for hydrocarbon reservoirs. Geo-Marine Letters. Vol 26, Issue 361. https://doi.org/10.1007/s00367-006-0047-x

Miller, K.G., Kominz, M.A., Browning, J.V., Wright, J.D., Mountain, G.S., Katz, M.E., Sugarman, P.J., Cramer, B.S., Christie-Blick, N., Pekar, S.F., 2005. The Phanerozoic record of global sea-level change. Science. Vol 310, Issue 5762, 1293-1298. http://dx.doi.org/10.1126/science.1116412

Milliman, J.D., Syvitski, J.P., 1992. Geomorphic/tectonic control of sediment discharge to the ocean: the importance of small mountainous rivers. The Journal of Geology. Vol 100, No. 5, 525-544.

Miramontes, E., Eggenhuisen, J.T., Silva Jacinto, R., Poneti, G., Pohl, F., Normandeau, A., Campbell, D.C., Hernández-Molina, F.J., 2020. Channel-levee evolution in combined contour current–turbidity current flows from flume-tank experiments. Geology. https://doi.org/10.1130/G47111.1

Miramontes, E., Jorry, S.J., Jouet, G., Counts, J.W., Courgeon, S., Le Roy, P., Guerin, C., Hernández-Molina, F.J., 2019b. Deep marine dunes on drowned isolated carbonate terraces (Mozambique Channel, SW Indian Ocean). Sedimentology. http://dx.doi.org/10.1111/sed.12572

Miramontes, E., Penven, P., Fierens, R., Droz, L., Toucanne, S., Jorry, S.J., Jouet, G., Pastor, L., Silva Jacinto, R., Gaillot, A., Giraudeau, J., Raisson, F., 2019a. The influence of bottom currents on the Zambezi Valley morphology (Mozambique Channel, SW Indian Ocean): In situ current observations and hydrodynamic modelling. Marine Geology. Vol 410, 42-55. http://dx.doi.org/10.1016/j.margeo.2019.01.002

Moore, A., 1999. A reappraisal of epeirogenic flexure axes in southern Africa. South African Journal of Geology. Vol 102, Issue 4, 363-376.

Mosher, D.C., Campbell, D.C., Gardner, J.V., Piper, J.W., Chavtor, J.D., Rebesco, M., 2017. The role of deep-water sedimentary processes in shaping a continental margin: The Northwest Atlantic. Marine Geology. Vol 393, 245-259. http://dx.doi.org/10.1016/j.margeo.2017.08.018

Mougenot, D., Recq, M., Virlogeux, P., Lepvrier, C., 1986. Seaward extension of the East African Rift. Nature. Vol 321, 599-603. http://dx.doi.org/10.1038/321599a0

Mueller, C.O., Jokat, W., 2017. Geophysical evidence for the crustal variation and distribution of magmatism along the central coast of Mozambique. Tectonophysics. Vol 712-713, 684-703. http://dx.doi.org/10.1016/j.tecto.2017.06.007

Mueller, C.O., Jokat, W., Schreckenberger, B., 2016. The crustal structure of Beira High, central Mozambique-Combined investigation of wide-angle seismic and potential field data. Tectonophysics. Vol 683, 233-254. http://dx.doi.org/10.1016/j.tecto.2016.06.028

Murphy, D.P., Thomas, D.J., 2012. Cretaceous deep-water formation in the Indian sector of the Southern Ocean. Paleoceanography and Paleoclimatology. Vol 27, Issue 1. http://dx.doi.org/10.1029/2011PA002198

Mutti, E., Normark, W.R., 1991. An integrated approach to the study of turbidite systems. In: Weimer, P., Link, H. (Eds.), Seismic Facies and Sedimentary Processes of Submarine Fans and Turbidite Systems. Springer, New York, pp. 75-106.

Nairn, A.E., Lerche, I., Iliffe, J. E., 1991. Geology, basin analysis, and hydrocarbon potential of Mozambique and the Mozambique Channel. Earth-Science Reviews. Vol 30, Issue 1, 81-123. http://dx.doi.org/10.1016/0012-8252(91)90014-7

Niemi, T.M., Ben-avraham, Z., Hartnady, C.J.H., Reznikov, M., 2000. Post-Eocene seismic stratigraphy of the deep ocean basin adjacent to the southeast African continental margin: a record of geostrophic bottom current systems. Marine Geology. Vol 162, Issue 2-4, 237-258. http://dx.doi.org/10.1016/S0025-3227(99)00062-6

Ogg, J.G., Ogg, G.M., Gradstein, F.M., 2016. A Concise Geologic Time Scale. Elsevier. 240 pp. http://dx.doi.org/10.1016/C2009-0-64442-1

Pekar, S.F., DeConto, R.M., Harwood, D.M., 2006. Resolving a late Oligocene conundrum: Deep-sea warming and Antarctic glaciation. Palaeogeography, Palaeoclimatology, Palaeoecology. Vol 231, Issues 1-2, 29-40. https://doi.org/10.1016/j.palaeo.2005.07.024

Pierce, E.L., van de Flierdt, T., Williams, T., Hemming, S.R., Cook, C.P., Passchier, S., 2017. Evidence for a dynamic East Antarctic ice sheet during the mid-Miocene climate transition. Earth and Planetary science Letters. Vol 478, 1-13. http://dx.doi.org/10.1016/j.epsl.2017.08.011

Polteau, S., Mazzini, A., Galland, O., Planke, S., Malthe-Sorenssen, A., 2008. Saucer-shaped intrusions: Occurences, emplacement and implications. Earth and Planetary Science Letters. Vol 266, 195-204. http://dx.doi.org/10.1016/j.epsl.2007.11.015

Ponte, J.P., 2018. La marge africaine du canal du Mozambique (le système turbiditique du Zambèze): une approche “Source to Sink” au Méso-Cénozoïque. Sciences de la Terre. Université Rennes 1, 2018. Français. ⟨NNT : 2018REN1B005⟩. ⟨tel-01865479⟩. 353 pp.

Ponte, J.P., Robin, C., Guillocheau, F., Popescu, S., Suc, J.P., Dall’Asta, M., Melinte-Dobrinescu, M.C., Bubik, M., Dupont, G., Gaillot, J., 2018. The Zambezi delta (Mozambique channel, East Africa): High resolution dating combining bio-orbital and seismic stratigraphy to determine climate (palaeoprecipitation) and tectonic controls on a passive margin. Marine and Petroleum Geology. http://dx.doi.org/10.1016/j.marpetgeo.2018.07.017

Potter, P.E., Szatmari, P., 2009. Global Miocene tectonics and the modern world. Earth-Science Reviews. Vol 96, 279-295. http://dx.doi.org/10.1016/j.earscirev.2009.07.003

Poulsen, C.J., Barron, E.J., Arthur, M.A., Peterson, W.H., 2001. Response of the Mid- Cretaceous global oceanic circulation to tectonic and CO2 forcings. Paleoceanography and Paleoclimatology. Vol 16, Issue 6, 576-592. http://dx.doi.org/10.1029/2000PA000579

Poulsen, C.J., Gendaszek, A.S., Jacob, R.L., 2003. Did the rifting of the Atlantic Ocean cause the Cretaceous thermal maximum? Geology. Vol 31, Issue 2, 115-118. http://dx.doi.org/10.1130/0091-7613(2003)031<0115:DTROTA>2.0.CO;2

Preu, B., Spieß, V., Schwenk, T., Schneider, R., 2011. Evidence for current-controlled sedimentation along the southern Mozambique continental margin since Early Miocene times. Geo-Marine Letters. Vol 31, Issue 5-6, 427-435. http://dx.doi.org/10.1007/s00367-011-0238-y

Read, J.F., Pollard, R.T., 1999. Deep inflow into the Mozambique Basin. Journal of Geophysical Research: Oceans. Vol 104, Issue C2, 3075-3090. http://dx.doi.org/10.1029/1998JC900078

Rebesco, M., 2005. Contourites. In: Selley, R.C., Cocks, L.R.M., Plimer, I.R. (Eds.), Encyclopedia of Geology. Oxford: Elsevier, 513-527. ISBN: 978-0-12-369396-9

Rebesco, M., Hernández-Molina, F.J., van Rooij, D., Wåhlin, A., 2014. Contourites and associated sediments controlled by deep-water circulation processes: state-of-the-art and future considerations. Marine Geology. Vol 352, 111-154. http://dx.doi.org/10.1016/j.margeo.2014.03.011

Rebesco, M., Mosher, D., Piper, D.J.W., 2017. Advancements in Understanding Deep-Sea Clastic Sedimentation Processes: a preface. Marine Geology. Vol 393, 1-3. http://dx.doi.org/10.1016/j.margeo.2017.10.007

Rebesco, M., Stow, D., 2001. Seismic expression of contourites and related deposits: a preface. Marine Geophysical Research. Vol 22, Issue 5-6, 303-308. http://dx.doi.org/10.1023/A:1016316913639

Robinson, S.A., Murphy, D.P., Vance, D., Thomas, D.J., 2010. Formation of “Southern Component Water” in the Late Cretaceous: Evidence from Nd-isotopes. Geology, Vol 38, Issue 10, 871-874. http://dx.doi.org/10.1130/G31165.1

Rodrigues, S., Hernández-Molina, F.J., Rodriguez, K., Hodgson, N., 2019. Late Cretaceous hybrid (turbidite-contourite) system on the Argentine Margin: palaeoceanographic and conceptual implications. Abstract in the IAS Meeting 2019.

Sahagian, D., Pinous, O., Olferiev, A., Zakharov, V., 1996. Eustatic curve for the Middle Jurassic-Cretaceous based on Russian platform and Siberian stratigraphy: Zonal resolution. American Association of Petroleum Geologists Bulletin. Vol 80, Issue 9, 1433-1458.

Salman, G., Abdula, I., 1995. Development of the Mozambique and Ruvuma sedimentary basins, offshore Mozambique. Sedimentary Geology. Vol 96, Issue 1, 7-41. http://dx.doi.org/10.1016/0037-0738(95)00125-R

Sangree, J.B., Waylett, D.C., Frazier, D.E., Amery, G.B. y., Fennessy, W.J., 1978. Recognition of continental-slope seismic facies, offshore Texas-Louisiana. In: Bouma, A.H., Moore, G.T. y., Coleman, J.M. (Eds.), Framework, Facies, and Oil-Trapping Characteristics of the Upper Continental Margin. AAPG, Tulsa, Oklahoma, pp. 87-117.

Sangree, J.B., Widmier, J.M., 1979. Interpretation of depositional facies from seismic data. Geophysics. Vol 44, 131-160.

Sansom, P., 2018. Hybrid turbidite-contourite systems of the Tanzanian margin. Petroleum Geoscience. https://doi.org/10.1144/petgeo2018-044

Schlüter, P., Uenzelmann-Neben, G., 2007. Seismostratigraphic analysis of the Transkei Basin: a history of deep sea current controlled sedimentation. Marine Geology. Vol 240, 99-111. http://dx.doi.org/10.1016/j.margeo.2007.02.015

Schlüter, P., Uenzelmann-neben, G., 2008. Indications for bottom current activity since Eocene times: the climate and ocean gateway archive of the Transkei Basin, South Africa. Global and Planetary Change. Vol 60, Issues 3-4, 416-428. http://dx.doi.org/10.1016/j.gloplacha.2007.07.002

Schouten, M.W., de Ruijter, W.P.M., van Leeuwen, P.J., 2002. Upstream control of Agulhas ring shedding. Journal of Geophysical Research: Oceans. Vol 107, Issue C8, 23-1–23-11. http://dx.doi.org/10.1029/2001JC000804

Schouten, M.W., de Ruijter, W.P.M., van Leeuwen, P.J., Ridderinkhof, H., 2003. Eddies and variability in the Mozambique Channel. Deep-Sea Research Part II: Tropical Studies in Oceanography. Vol 50, Issue 12-13, 1987-2003. http://dx.doi.org/10.1016/S0967-0645(03)00042-0

Senkans, A., Leroy, S., d'Acremont, E., Castilla, R., Despinois, F., 2019. Polyphase rifting and break-up of the central Mozambique margin. Marine and Petroleum Geology. Vol 100, 412-433. http://dx.doi.org/10.1016/j.marpetgeo.2018.10.035

Shipp, R.C., Weimer, P., Posamentier, H.W., 2011. Mass- Transport Deposits in Deepwater Settings: An Introduction. In: Shipp, R.C., Weimer, P., Posamentier, H.W. (Eds.), Mass- Transport Deposits in Deepwater Settings. SEPM Society for Sedimentary Geology, Vol 96. https://doi.org/10.2110/sepmsp.096.003

Siedler, G., Rouault, M., Biastoch, A., Backeberg, B., Reason, C.J.C., Lutjeharms, J.R.E., 2009. Modes of the southern extension of the East Madagascar Current. Journal of Geophysical Research: Oceans. Vol 114 (C01005), 1-15. http://dx.doi.org/10.1029/2008JC004921

Simpson, E.S.W., Schlich, R., Gieskes, J., Girdley, W.A., Leclaire, L., Marshall, B.V., Moore, C., Müller, C., Sigal, J., Vallier, T.L., White, S.M., Zobel, B., 1974a. Site 248. In: Simpson, E.S.W., Schlich, R., Gieskes, J., Girdley, W.A., Leclaire, L., Marshall, B.V., Moore, C., Müller, C., Sigal, J., Vallier, T.L., White, S.M., Zobel, B. (Eds.), Initial Reports of the Deep Sea Drilling Project. Washington (U.S. Government Printing Office). Vol 25, 259-286. http://doi.org/10.2973/dsdp.proc.25.109.1974

Simpson, E.S.W., Schlich, R., Gieskes, J., Girdley, W.A., Leclaire, L., Marshall, B.V., Moore, C., Müller, C., Sigal, J., Vallier, T.L., White, S.M., Zobel, B., 1974b. Site 249. In: Simpson, E.S.W., Schlich, R., Gieskes, J., Girdley, W.A., Leclaire, L., Marshall, B.V., Moore, C., Müller, C., Sigal, J., Vallier, T.L., White, S.M., Zobel, B. (Eds.), Initial Reports of the Deep Sea Drilling Project. Washington (U.S. Government Printing Office). Vol 25, 287-346. http://doi.org/10.2973/dsdp.proc.25.110.1974

Sinha, M.C., Louden, K.E., Parsons, B., 1981. The crustal structure of the Madagascar Ridge. Geophysical Journal International. Vol 66, Issue 2, 351-377. http://dx.doi.org/10.1111/j.1365-246X.1981.tb05960.x

Stow, D.A.V., Hernández-Molina, F.J., Llave, E., Sayago, M., Díaz del Río, V., Branson, A., 2009. Bedform-velocity matrix: the estimation of bottom current velocity from bedform observations. Geology. Vol 37, Issue 4, 327-330. http://dx.doi.org/10.1130/G25259A.1

Stow, D.A.V., Hunter, S., Wilkinson, D., Hernández-Molina, F.J., 2008. The nature of contourite deposition. In: Rebesco, M., Camerlenghi, A. (Eds.), Contourites. Developments in Sedimentology. Vol 60. Elsevier, pp. 143-156.

Swart, N.C., Lutjeharms, J.R.E., Ridderinkhof, H., de Ruijter, W.P.M., 2010. Observed characteristics of Mozambique Channel eddies. Journal of Geophysical Research. Vol 115 (C09006), 1-14. http://dx.doi.org/10.1029/2009JC005875

Thieblemont, A., Hernández-Molina, F.J., Miramontes, E., Raisson, F., Penven, P., 2019. Contourite depositional systems along the Mozambique Channel: the interplay between bottom currents and sedimentary processes. Deep-Sea Research Part 1: Oceanographic Research Papers. Vol 147, 79-99. http://dx.doi.org/10.1016/j.dsr.2019.03.012

Thomas, D.J., Bralower, T.J., Jones, C.E., 2003. Neodymium isotopic reconstruction of late Paleocene-early Eocene thermohaline circulation. Earth and Planetary Science Letters. Vol 209, Issues 3-4, 309-322. http://dx.doi.org/10.1016/S0012-821X(03)00096-7

Toole, J.M., Warren, B.A., 1993. A hydrographic section across the subtropical South Indian Ocean. Deep-Sea Research Part I: Oceanographic Research Papers. Vol 40, Issue 10, 1973-2019. http://dx.doi.org/10.1016/0967-0637(93)90042-2

Tucholke, B.E., Carpenter, G.B., 1977. Sediment distribution and Cenozoic sedimentation patterns on the Agulhas plateau. Geological Society of America Bulletin. Vol 88, Issue 9, 1337-1346. http://dx.doi.org/10.1130/0016-7606(1977)88<1337:SDACSP>2.0.CO;2

Tucholke, B.E., Embley, R.W., 1984. Cenozoic regional erosion of the abyssal sea floor off South Africa. In: Schlee, J.S. (Eds.), Interregional Unconformities and Hydrocarbon Accumulation. American Association of Petroleum Geologists. Vol 36. http://dx.doi.org/10.1306/M36440C11

Uenzelmann-Neben, G. and Huhn, K., 2009. Sedimentary deposits on the southern South African continental margin: Slumping versus non deposition or erosion by oceanic currents? Marine Geology. Vol 266, 6-79. http://dx.doi.org/10.2113/gssajg.114.3-4.449

Uenzelmann-Neben, G., 2001. Seismic characteristics of sediment drifts: An example from the Agulhas Plateau, southwest Indian Ocean. Marine Geophysical Research. Vol 22, Issue 5-6, 323-343. http://dx.doi.org/10.1023/A:1016391314547

Uenzelmann-Neben, G., 2002. Contourites on the Agulhas plateau, SW Indian Ocean: indications for the evolution of currents since Palaeogene times. Geological Society, London, Memoirs. Vol 22, 271-288. http://dx.doi.org/10.1144/GSL.MEM.2002.022.01.20

Uenzelmann-Neben, G., Schlüter, P., Weigelt, E., 2007. Cenozoic oceanic circulation within the South African gateway: indications from seismic stratigraphy. South African Journal of Geology. Vol 110, 275-294. http://dx.doi.org/10.2113/gssajg.110.2-3.275

Uenzelmann-neben, G., Watkeys, M.K., Kretzinger, W., Frank, M., Heuer, L., 2011. Paleoceanogrpahic interpretation of a seismic profile from the southern Mozambique ridge, southwestern Indian ocean. South African Journal of Geology. Vol 114, Issue 3-4, 449-458. http://dx.doi.org/10.2113/gssajg.114.3-4.449

Uenzelmann-Neben, G., Weber, T., Grützner, J., Thomas, M., 2017. Transition from the Cretaceous ocean to Cenozoic circulation in the western South Atlantic - a twofold reconstruction. Tectonophysics. Vol 716, 225-240 http://dx.doi.org/10.1016/j.tecto.2016.05.036

Ullgren, J.E., van Aken, H.M., Ridderinkohof, H., de Ruijter, W.P.M., 2012. The hydrography of the Mozambique Channel from six years of continuous temperature, salinity, and velocity observations. Deep Sea Research Part I: Oceanographic Research Papers. Vol 69, 36-50. http://dx.doi.org/10.1016/j.dsr.2012.07.003

Vallier, T.L., 1974. Volcanogenic Sediments and Their Relation to Landmass Volcanism and Sea Floor-Continent Movements, Western Indian Ocean, Leg 25, Deep Sea Drilling Project. DSDP Vol 25. Part II, 21, 515-542. http://dx.doi.org/10.2973/dsdp.proc.25.121.1974

van Aken, H.M., Ridderinkhof, H., de Ruijter, W.P.M., 2004. North Atlantic deep water in the south-western Indian Ocean. Deep Sea Research Part I: Oceanographic Research Papers. Vol 51, Issue 6, 755-776. http://dx.doi.org/10.1016/j.dsr.2004.01.008

Viana, A.R., Almeida Jr., W., Nunes, M.C.V., Bulhões, E.M., 2007. The economic importance of contourites. Geological Society, London, Special Publication, 276, 1-23. http://dx.doi.org/10.1144/GSL.SP.2007.276.01.01

Voigt, S., Jung, C., Friedrich, O., Frank, M., Teschner, C., Hoffmann, J., 2013. Tectonically restricted deep-ocean circulation at the end of the Cretaceous greenhouse. Earth and Planetary Science Letters. Vol 369-370, 169-177. http://dx.doi.org/10.1016/j.epsl.2013.03.019

Walford, H.L., White, N.J., Sydow, J.C., 2005. Solid sediment load history of the Zambezi Delta. Earth and Planetary Science Letters. Vol 238, Issues 1-2, 49-63. http://dx.doi.org/10.1016/j.epsl.2005.07.014

Weatherall, P., Marks, K. M., Jakobsson, M., Schmitt, T., Tani, S., Arndt, J. E., Rovere, M., Chayes, D., Ferrini, V., Wigley, R., 2015. A new digital bathymetric model of the world's oceans. Earth and Space Science. Vol 2, Issue 8, 331-345. http://doi.org/10.1002/2015EA000107

Wiles, E., Green, A., Watkeys, M., Jokat, W., Krocker, R., 2014. A new pathway for Deep water exchange between the Natal Valley and Mozambique Basin? Geo-Marine Letters. Vol 34, Issue 6, 525-540. http://dx.doi.org/10.1007/s00367-014-0383-1

Wiles, E., Green, A.N., Watkeys, M.K., Jokat, W., 2017. Zambezi continental margin: compartmentalized sediment transfer routes to the abyssal Mozambique Channel. Marine Geophysical Research. Vol 38, Issue 3, 227-240. http://dx.doi.org/10.1007/s11001-016-9301-4

Wynn, R.B., Stow, D.A.V., 2002. Classification and characterisation of deep-water sediment waves. Marine Geology. Vol 192, 7-22. http://dx.doi.org/10.1016/S0025-3227(02)00547-9

Wyrtki, K., 1973. Physical oceanography in the Indian Ocean. In: Zeitzschel, B., Gerlach, S.A. (Eds.), The Biology of the Indian Ocean. Ecological Studies (Analysis and Synthesis), Vol 3. Springer, Berlin, Heidelberg, 18-36. ISBN: 978-3-642-65468-8. http://dx.doi.org/10.1007/978-3-642-65468-8_3

You, Y., 1997. Seasonal variations of thermocline circulation and ventilation in the Indian Ocean. Journal of Geophysical Research: Oceans. Vol 102, Issue C5, 10,391-10,422. http://dx.doi.org/10.1029/96JC03600

You, Y., 1999. Dianeutral, mixing transformation and transport of the deep water of the Indian Ocean. Deep-Sea Research Part I: Oceanographic Research Papers. Vol 46, Issue 1, 109-148. http://dx.doi.org/10.1016/S0967-0637(98)00058-2

Zachos, J.C., Pagani, M., Sloan, L., Thomas, E., Billups, K., 2001. Trends, rhythms and aberrations in global climate 65 Ma to present. Science. Vol 292, 686-693. http://dx.doi.org/10.1126/science.1059412

Highlights

- Late Cretaceous to Cenozoic evolution off the Mozambique Channel, SW Indian Ocean
- Onset of contourite depositional systems as early as Aptian-Albian time
- Major shifts in sedimentary evolution at late Cenomanian, late Oligocene & 17-15 Ma
- Present morphosedimentary features were established around the early Pleistocene
- Tectonic, climate, glacial & palaeoceanographic events influenced margin deposition

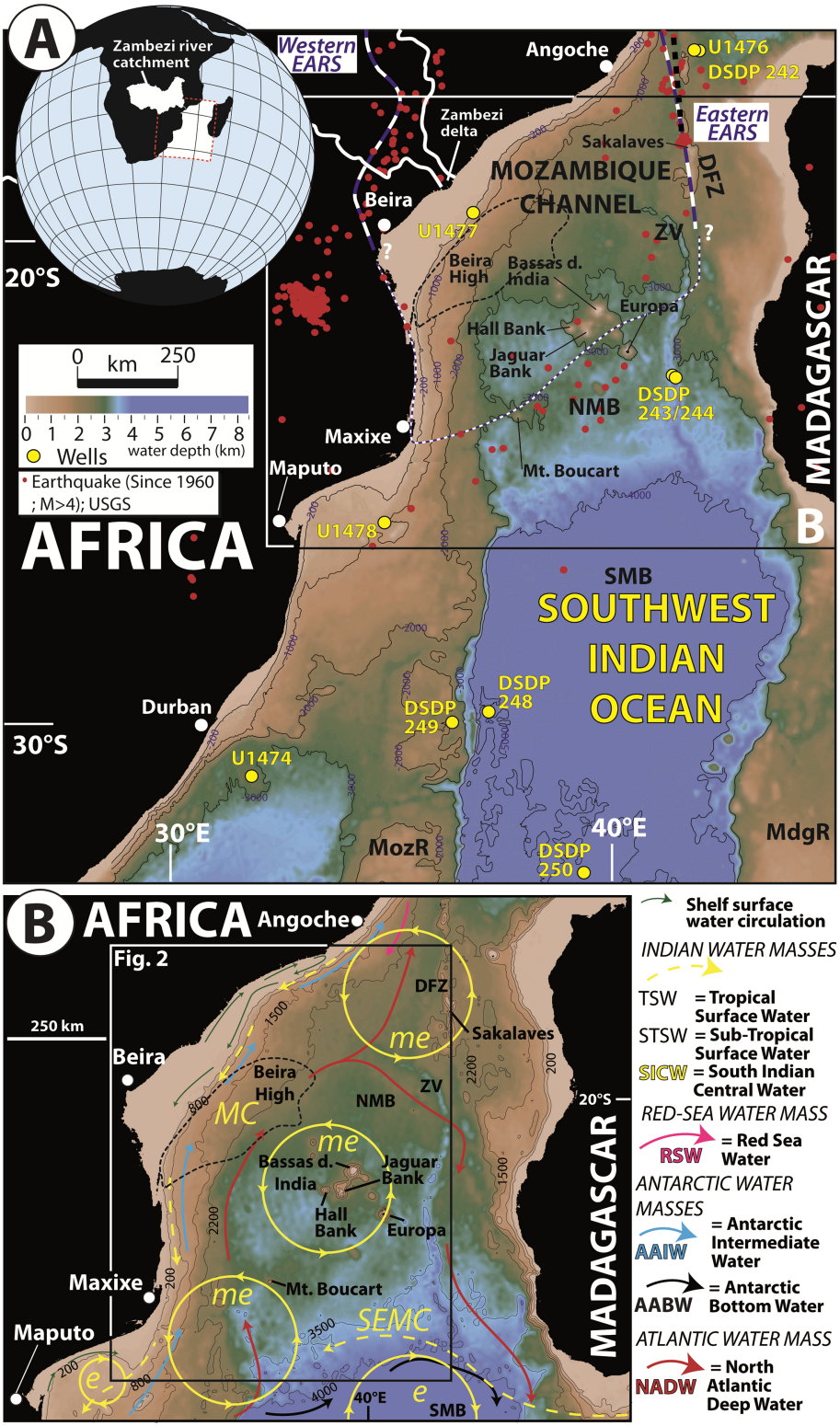
A
Zambezi river catchment
Western EARS
Angoche
U1476
DSDP 242
Eastern EARS
Zambezi delta
Sakalaves
DFZ
MOZAMBIQUE CHANNEL
Beira
U1477
ZV
20°S
Beira High
Bassas d. India
Europa
Hall Bank
Jaguar Bank
MADAGASCAR
0 km 250
0 1 2 3 4 5 6 7 8
water depth (km)
Wells
Earthquake (Since 1960 ; M>4); USGS
DSDP 243/244
NMB
Maxixe
Maputo
Mt. Boucart
AFRICA
U1478
B
SMB
SOUTHWEST INDIAN OCEAN
DSDP 248
DSDP 249
Durban
30°S
U1474
30°E
MozR
40°E
DSDP 250
MdgR

B AFRICA
Angoche
Fig. 2
250 km
DFZ
me
Sakalaves
Beira
Beira High
ZV
NMB
MC
20°S
MADAGASCAR
Bassas d. India
Jaguar Bank
Hall Bank
Europa
Maxixe
Mt. Boucart
SEMC
Maputo
e
40°E
SMB
Shelf surface water circulation
INDIAN WATER MASSES
TSW = Tropical Surface Water
STSW = Sub-Tropical Surface Water
SICW = South Indian Central Water
RED-SEA WATER MASS
RSW = Red Sea Water
ANTARCTIC WATER MASSES
AAIW = Antarctic Intermediate Water
AABW = Antarctic Bottom Water
ATLANTIC WATER MASS
NADW = North Atlantic Deep Water

Figure 1

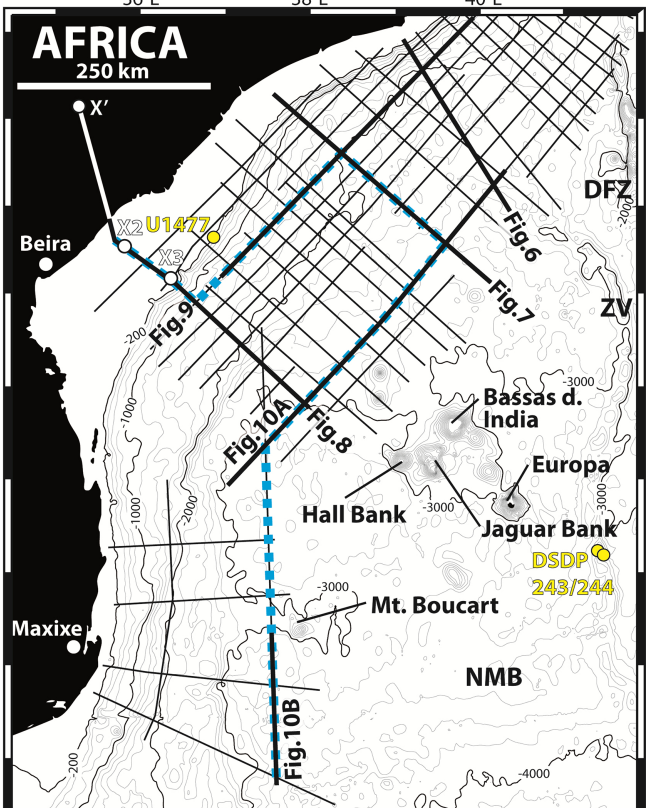

Seismic lines (*INP & WesternGeco*)

Exploration wells

DSPD Leg 25 & IODP Exp. 361

Selected 2D multichannel seismic lines

Regional 2D multichannel seismic line in **Fig. 3**

Figure 2

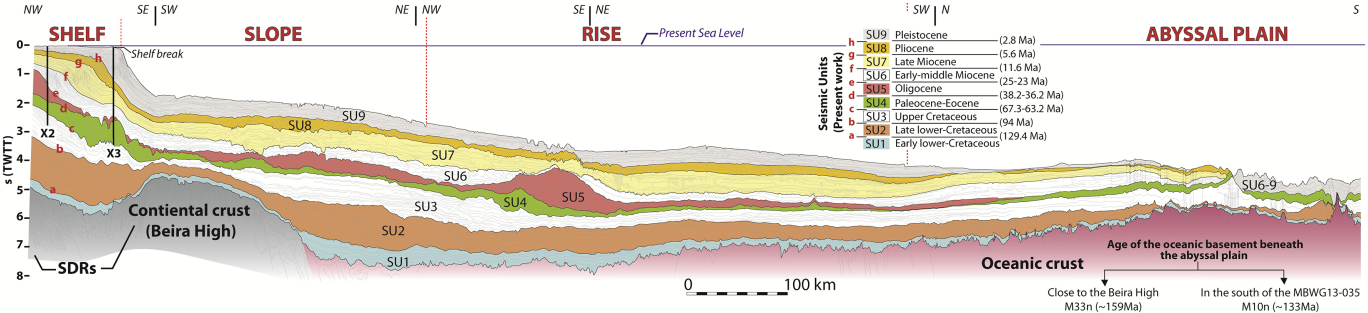
NW
SE | SW
NE | NW
SE | NE
SW | N
S
SHELF
SLOPE
RISE
ABYSSAL PLAIN
Present Sea Level
Shelf break
s (TWTT)
0
1
2
3
4
5
6
7
8
X2
X3
SU9
SU8
SU7
SU6
SU5
SU4
SU3
SU2
SU1
SU6-9
Contiental crust
(Beira High)
SDRs
Oceanic crust
0
100 km
Seismic Units
(Present work)
h SU9 Pleistocene (2.8 Ma)
g SU8 Pliocene (5.6 Ma)
f SU7 Late Miocene (11.6 Ma)
e SU6 Early-middle Miocene (25-23 Ma)
d SU5 Oligocene (38.2-36.2 Ma)
c SU4 Paleocene-Eocene (67.3-63.2 Ma)
b SU3 Upper Cretaceous (94 Ma)
a SU2 Late lower-Cretaceous (129.4 Ma)
SU1 Early lower-Cretaceous
Age of the oceanic basement beneath the abyssal plain
Close to the Beira High
M33n (~159Ma)
In the south of the MBWG13-035
M10n (~133Ma)

Figure 3

SEISMIC FACIES TEMPLATE

Types	Seismic sections	Schematic facies geometries	Seismic facies	Depositional element
Prograding clinoforms	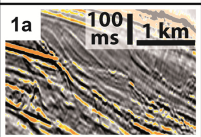	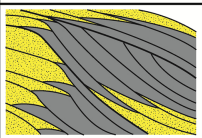	Mixture of low to high acoustic response seismic reflections with a complex sigmoidal/oblique internal reflection pattern.	Shelf prograding features
Disrupted	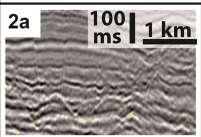	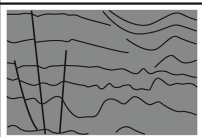	Disrupted, low acoustic response seismic reflections, with flat top and base surfaces.	Hemipelagites
Parallel/ sub-parallel	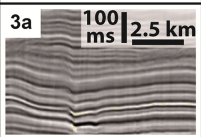	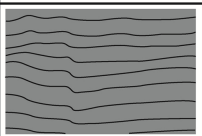	Fair continuity, parallel low acoustic response seismic reflections with flat base and top surfaces.	
	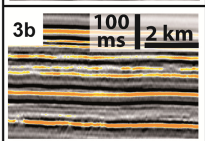	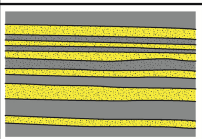	Fair continuity, sub-parallel high acoustic response seismic reflections, with non erosive, oblique top and base surfaces.	Heterogeneous density current features: ■ Levees ■ Sedimentary lobes ■ Channels
Hummocky	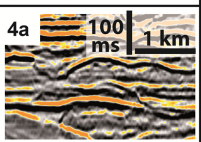	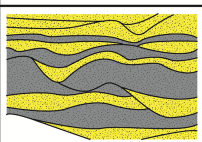	High acoustic response seismic reflections, lens-shaped external form with non-erosive, oblique top and base surfaces.	Sedimentary lobes
Chaotic	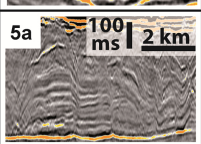	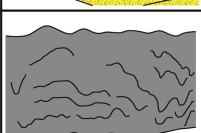	Chaotic, low to moderate acoustic response seismic reflections, lenticular shaped external form with an erosional base and irregular convex top boundary.	MTDs
	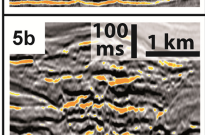	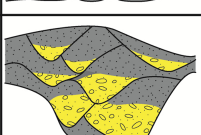	Chaotic, high acoustic response seismic reflections, «bowl» shaped external form with an erosional base.	Downslope channels

Figure 4

SEISMIC FACIES TEMPLATE FOR CDS

Types	Seismic sections	Schematic facies geometries	Seismic facies	Seismic units
LARGE CONTOURITE DRIFTS				
Prograding clinoforms	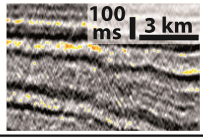	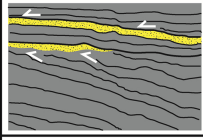	Low acoustic response seismic reflections with parallel/tangential oblique internal reflection pattern. Mounded external form. Local high acoustic response seismic reflections.	Seismic unit 2 (Beira drift)
Disrupted	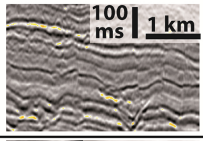	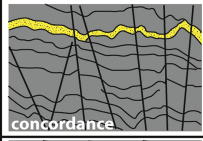	Disrupted, low acoustic response seismic reflections. Mounded external form. Local high acoustic response seismic reflections.	Seismic units 6 and 7 (Angoche drift)
Parallel/ sub-parallel	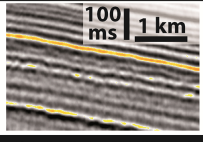	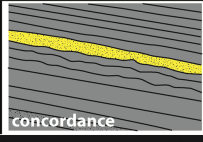	High continuity, parallel/sub-parallel low acoustic response seismic reflections. Mounded external form. Local high acoustic response seismic reflections.	Seismic units 4 and 5 (Angoche drift) Seismic units 4, 5, and 6 (Zambezi drift) Seismic units 2, 3, and 4 (Limpopo drifts)
SMALL CONTOURITE DRIFTS (MIXED DRIFTS)				
Variable	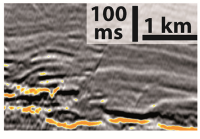	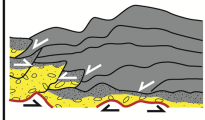	(*Drift*) High continuity parallel to disrupted low acoustic response seismic reflections. Mounded external form. (*Channel*) Chaotic, high acoustic response seismic reflections with U-shaped external form. Erosional base. Local MTDs (see facies 5a in **Fig. 4**).	Seismic unit 3 Seismic units 6 and 7
SEDIMENT WAVES				
Wavy	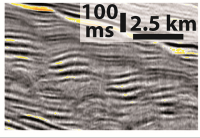	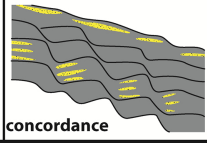	Wavy, low to moderate acoustic response seismic reflections, with a tabular external form.	Seismic units 3, 4, and 5 ■ Continental slope (SU3) ■ Continental rise (SU4) ■ Zambezi drift (SU4, SU5)
EROSIONAL FEATURES				
Variable	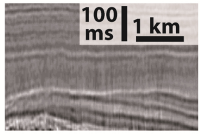	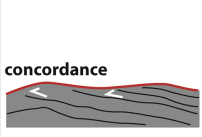	***Erosional surfaces:*** high continuity low to high acoustic response seismic reflection. Sheeted external form.	Top of seismic unit 2 Seismic unit 5 hiatus
	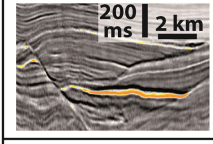	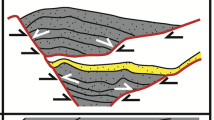	High continuity low to high acoustic response seismic reflection. «Bowl» shaped external form. ■ ***Contourite channels:*** fill by fair continuity low to moderate acoustic response seismic reflections. Linear along-slope trend. ■ ***Contourite moats:*** fill by high continuity low to moderate acoustic response seismic reflections. Linear along-slope trend adjacent to contourite drifts. ■ ***Scours:*** fill by high continuity low to moderate acoustic response seismic reflections and local MTDs (see facies 5a in **Fig. 4**). Sub-circular.	Seismic unit 5
	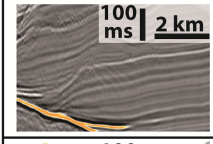	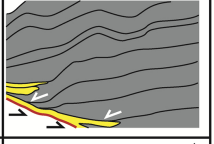		Seismic units 2, 3 and 4 (southern Limpopo drift)
	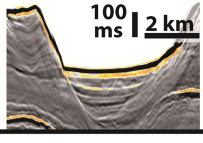	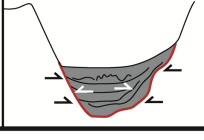		Seismic units 6 to 9

Figure 5

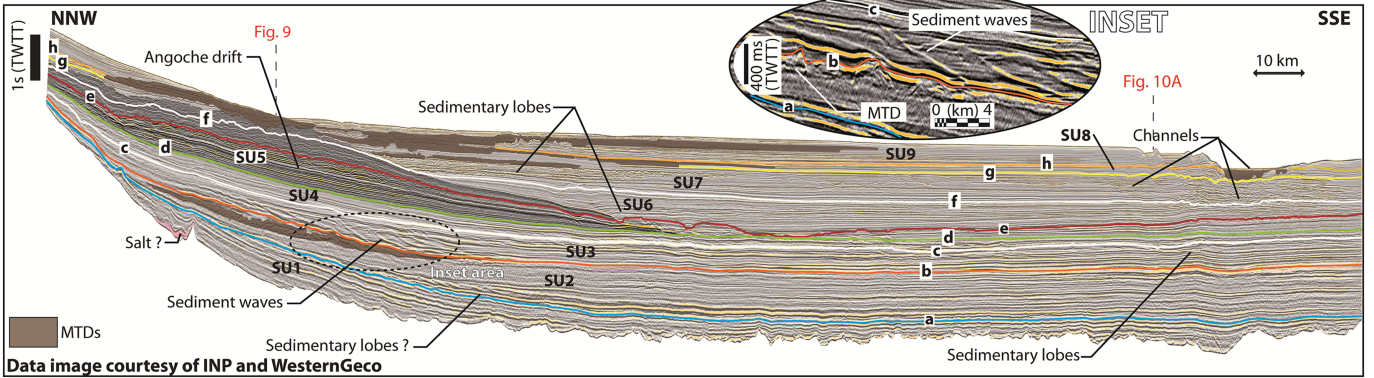
NNW
SSE
1s (TWTT)
Fig. 9
Angoche drift
Sedimentary lobes
INSET
Sediment waves
400 ms (TWTT)
MTD
0 (km) 4
10 km
Fig. 10A
SU8
Channels
SU9
SU7
SU6
SU5
SU4
SU3
SU2
SU1
Salt ?
Inset area
Sediment waves
Sedimentary lobes ?
Sedimentary lobes
MTDs
Data image courtesy of INP and WesternGeco

Figure 6

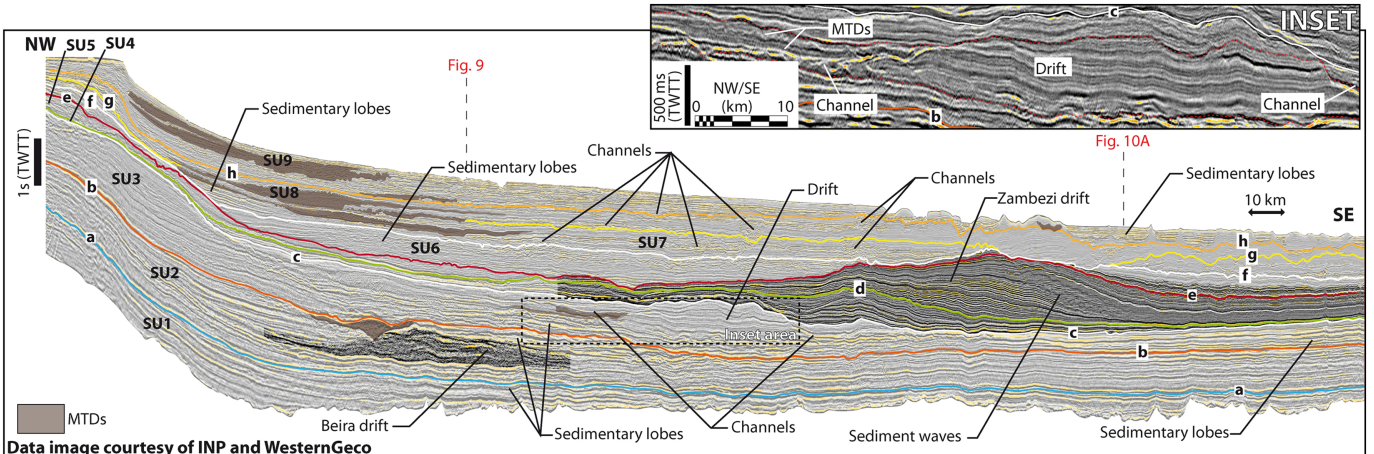
NW
SU5
SU4
e
f
g
1s (TWTT)
Sedimentary lobes
Fig. 9
h
SU9
SU8
b
SU3
a
SU2
SU1
c
SU6
Sedimentary lobes
Channels
SU7
Drift
Channels
Zambezi drift
Fig. 10A
Sedimentary lobes
10 km
SE
h
g
f
e
d
Inset area
c
b
a
MTDs
Beira drift
Sedimentary lobes
Channels
Sediment waves
Sedimentary lobes
Data image courtesy of INP and WesternGeco
INSET
MTDs
c
Drift
500 ms (TWTT)
NW/SE
0 (km) 10
Channel
b
Channel

Figure 7

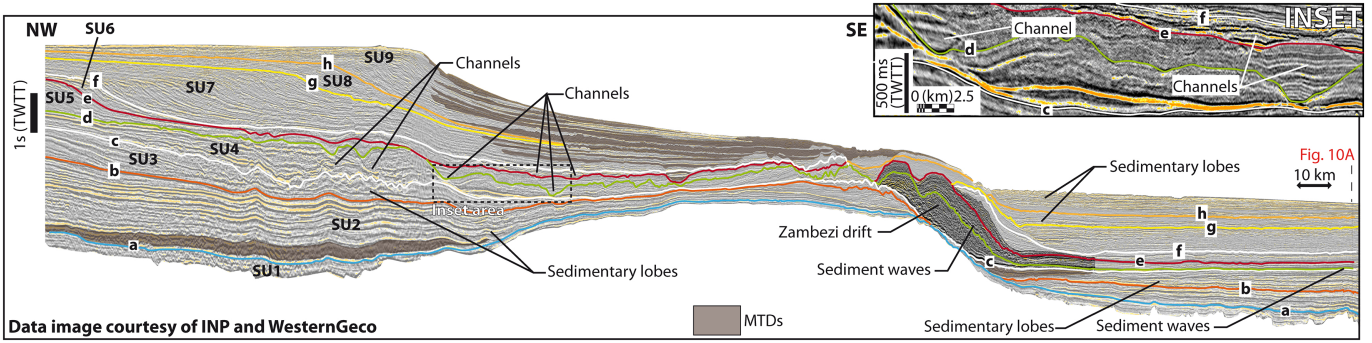
NW
SE
SU1
SU2
SU3
SU4
SU5
SU6
SU7
SU8
SU9
a
b
c
d
e
f
g
h
1s (TWTT)
Channels
Channels
Inset area
Sedimentary lobes
Zambezi drift
Sediment waves
Sedimentary lobes
Sediment waves
Sedimentary lobes
MTDs
Data image courtesy of INP and WesternGeco
INSET
Channel
Channels
500 ms (TWTT)
0 (km)2.5
Fig. 10A
10 km

Figure 8

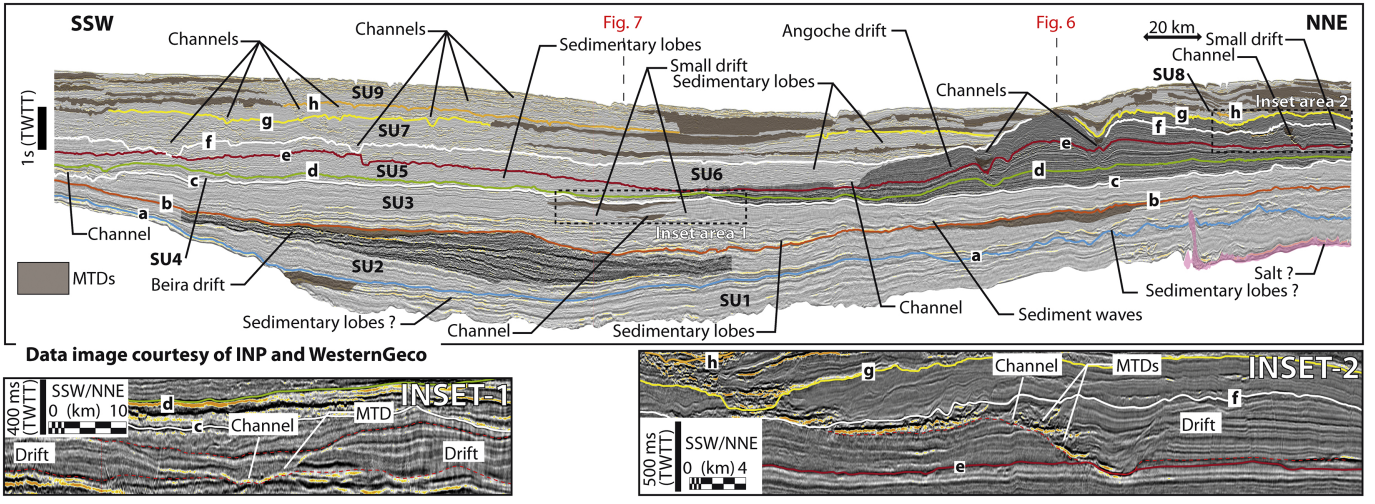
SSW
NNE
Fig. 7
Fig. 6
20 km
1s (TWTT)
Channels
Channels
Sedimentary lobes
Small drift
Sedimentary lobes
Angoche drift
Channels
Small drift
Channel
SU8
Inset area 2
SU9
SU7
SU5
SU6
SU3
SU4
SU2
SU1
MTDs
Channel
Beira drift
Sedimentary lobes ?
Channel
Inset area 1
Sedimentary lobes
Channel
Sediment waves
Salt ?
Sedimentary lobes ?
Data image courtesy of INP and WesternGeco
INSET-1
400 ms (TWTT)
SSW/NNE
0 (km) 10
Drift
Channel
MTD
Drift
INSET-2
500 ms (TWTT)
SSW/NNE
0 (km) 4
Channel
MTDs
Drift

Figure 9

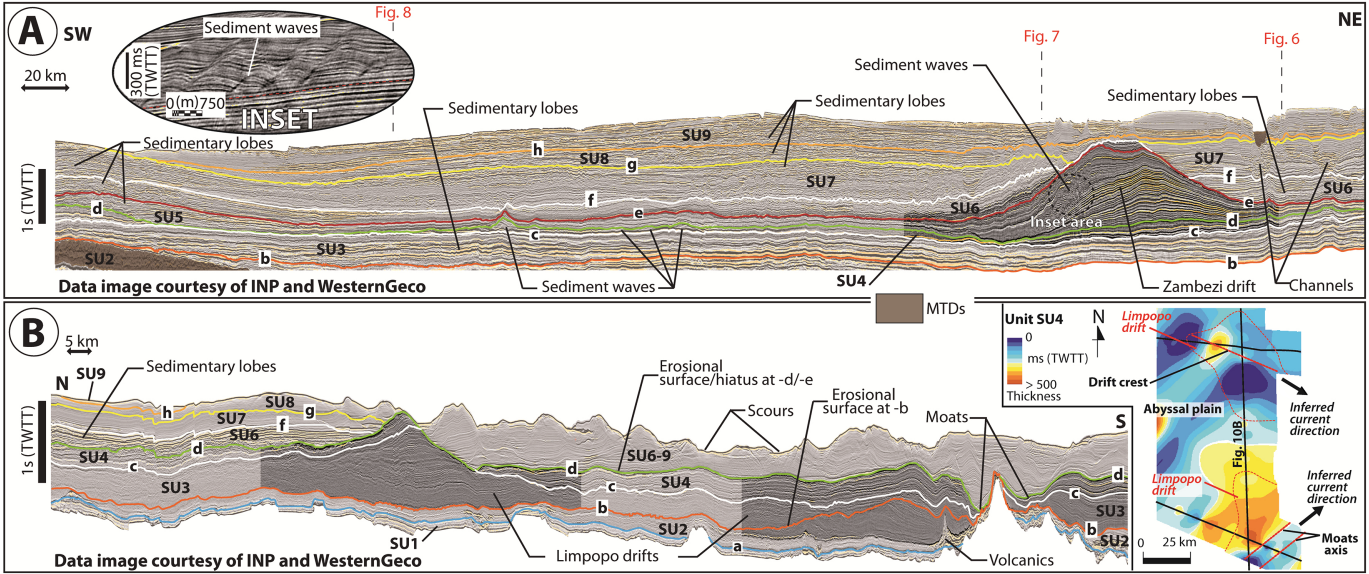
A
SW
NE
20 km
Sediment waves
300 ms (TWTT)
0 (m) 750
INSET
Fig. 8
Fig. 7
Fig. 6
Sedimentary lobes
Sediment waves
Sedimentary lobes
Sedimentary lobes
Sedimentary lobes
1s (TWTT)
SU2
SU3
SU4
SU5
SU6
SU7
SU8
SU9
Inset area
Zambezi drift
Channels
Sediment waves
Data image courtesy of INP and WesternGeco
MTDs
B
5 km
N
S
Sedimentary lobes
Erosional surface/hiatus at -d/-e
Scours
Erosional surface at -b
Moats
1s (TWTT)
SU1
SU2
SU3
SU4
SU6-9
SU6
SU7
SU8
SU9
Limpopo drifts
Volcanics
Data image courtesy of INP and WesternGeco
Unit SU4
0
ms (TWTT)
> 500
Thickness
N
Limpopo drift
Drift crest
Abyssal plain
Inferred current direction
Fig. 10B
Limpopo drift
Inferred current direction
Moats axis
0
25 km

Figure 10

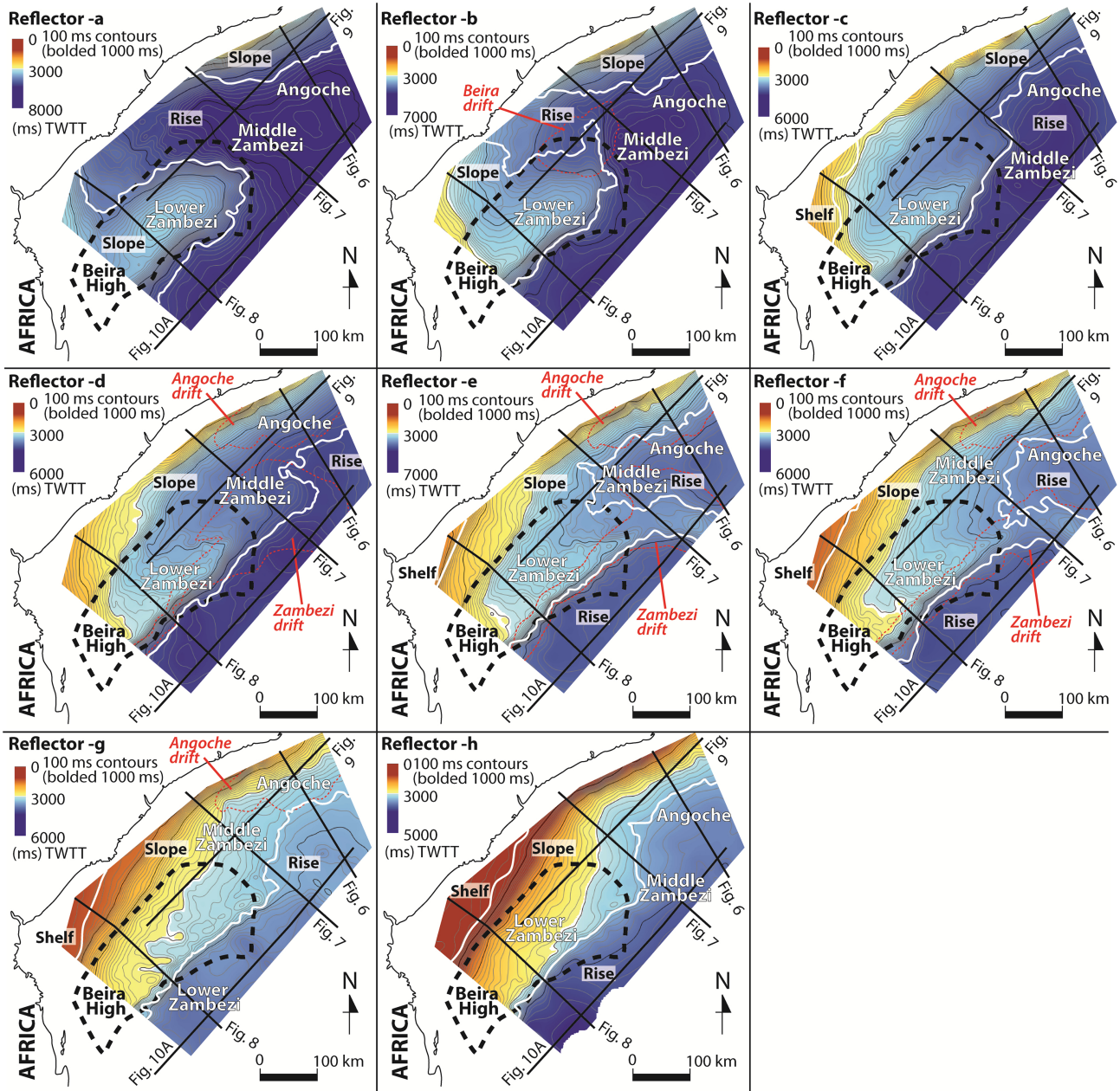
Reflector -a
0 100 ms contours (bolded 1000 ms)
3000
8000
(ms) TWTT
Slope
Angoche
Rise
Middle Zambezi
Lower Zambezi
Slope
Beira High
AFRICA
Fig. 9
Fig. 6
Fig. 7
Fig. 8
Fig. 10A
N
0
100 km
Reflector -b
0 100 ms contours (bolded 1000 ms)
3000
7000
(ms) TWTT
Beira drift
Slope
Angoche
Rise
Middle Zambezi
Slope
Lower Zambezi
Beira High
AFRICA
Reflector -c
0 100 ms contours (bolded 1000 ms)
3000
6000
(ms) TWTT
Slope
Angoche
Rise
Middle Zambezi
Shelf
Lower Zambezi
Beira High
AFRICA
Reflector -d
0 100 ms contours (bolded 1000 ms)
3000
6000
(ms) TWTT
Angoche drift
Angoche
Rise
Slope
Middle Zambezi
Lower Zambezi
Zambezi drift
Beira High
AFRICA
Reflector -e
0 100 ms contours (bolded 1000 ms)
3000
7000
(ms) TWTT
Angoche drift
Angoche
Slope
Middle Zambezi
Rise
Shelf
Lower Zambezi
Rise
Zambezi drift
Beira High
AFRICA
Reflector -f
0 100 ms contours (bolded 1000 ms)
3000
6000
(ms) TWTT
Angoche drift
Middle Zambezi
Angoche
Slope
Rise
Shelf
Lower Zambezi
Rise
Zambezi drift
Beira High
AFRICA
Reflector -g
0 100 ms contours (bolded 1000 ms)
3000
6000
(ms) TWTT
Angoche drift
Angoche
Middle Zambezi
Slope
Rise
Shelf
Lower Zambezi
Beira High
AFRICA
Reflector -h
0100 ms contours (bolded 1000 ms)
3000
5000
(ms) TWTT
Angoche
Slope
Shelf
Middle Zambezi
Lower Zambezi
Rise
Beira High
AFRICA

Figure 11

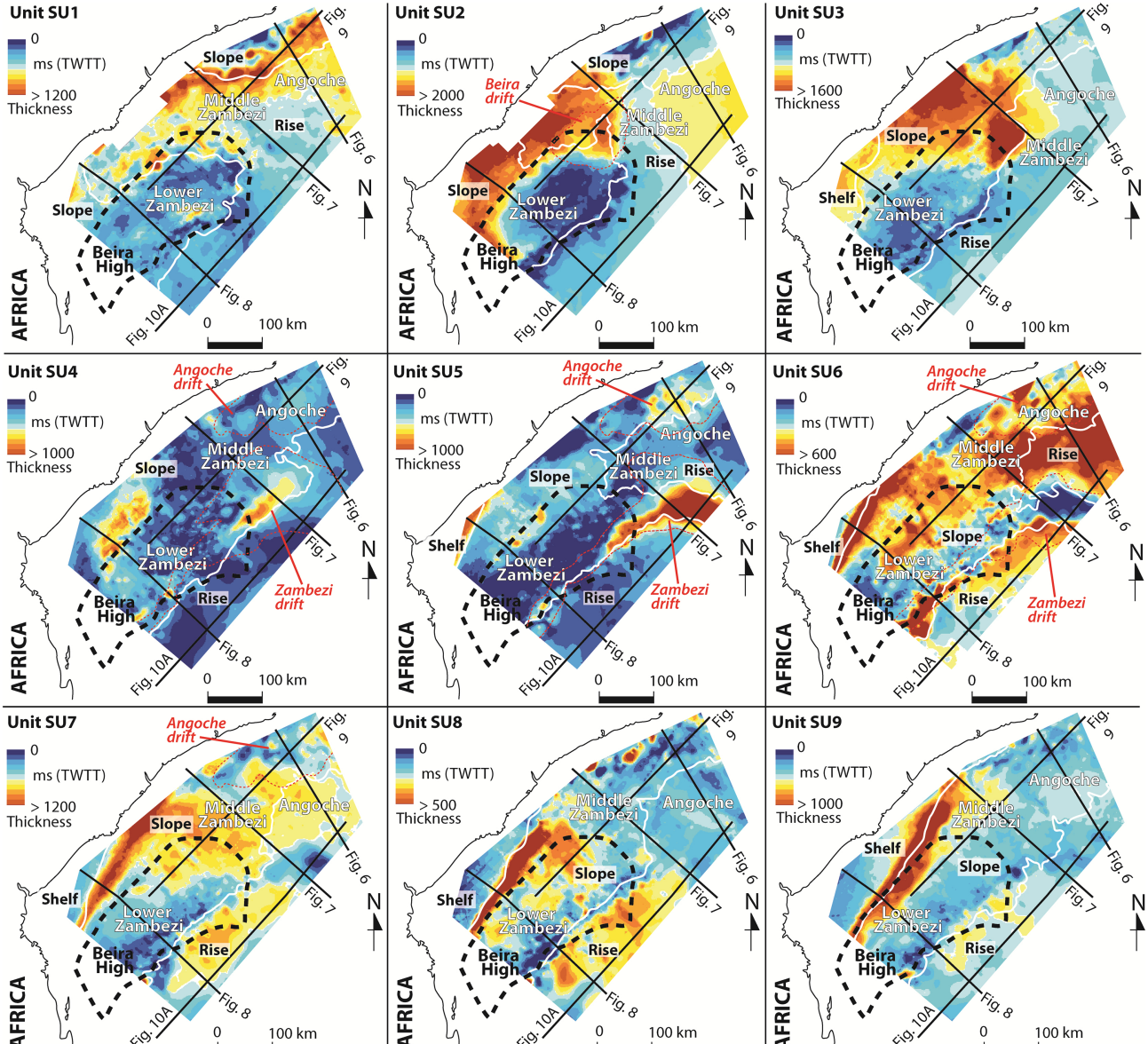
Unit SU1
0
ms (TWTT)
> 1200
Thickness
Slope
Angoche
Middle Zambezi
Rise
Lower Zambezi
Slope
Beira High
AFRICA
Fig. 9
Fig. 6
Fig. 7
Fig. 8
Fig. 10A
N
0
100 km
Unit SU2
0
ms (TWTT)
> 2000
Thickness
Beira drift
Slope
Angoche
Middle Zambezi
Rise
Slope
Lower Zambezi
Beira High
AFRICA
Fig. 9
Fig. 6
Fig. 7
Fig. 8
Fig. 10A
N
0
100 km
Unit SU3
0
ms (TWTT)
> 1600
Thickness
Angoche
Slope
Middle Zambezi
Shelf
Lower Zambezi
Rise
Beira High
AFRICA
Fig. 9
Fig. 6
Fig. 7
Fig. 8
Fig. 10A
N
0
100 km
Unit SU4
0
ms (TWTT)
> 1000
Thickness
Angoche drift
Angoche
Middle Zambezi
Slope
Lower Zambezi
Zambezi drift
Beira High
Rise
AFRICA
Fig. 9
Fig. 6
Fig. 7
Fig. 8
Fig. 10A
N
0
100 km
Unit SU5
0
ms (TWTT)
> 1000
Thickness
Angoche drift
Angoche
Middle Zambezi
Rise
Slope
Shelf
Lower Zambezi
Zambezi drift
Beira High
Rise
AFRICA
Fig. 9
Fig. 6
Fig. 7
Fig. 8
Fig. 10A
N
0
100 km
Unit SU6
0
ms (TWTT)
> 600
Thickness
Angoche drift
Angoche
Middle Zambezi
Rise
Shelf
Slope
Lower Zambezi
Zambezi drift
Beira High
Rise
AFRICA
Fig. 9
Fig. 6
Fig. 7
Fig. 8
Fig. 10A
N
0
100 km
Unit SU7
0
ms (TWTT)
> 1200
Thickness
Angoche drift
Slope
Middle Zambezi
Angoche
Shelf
Lower Zambezi
Rise
Beira High
AFRICA
Fig. 9
Fig. 6
Fig. 7
Fig. 8
Fig. 10A
N
0
100 km
Unit SU8
0
ms (TWTT)
> 500
Thickness
Middle Zambezi
Angoche
Slope
Shelf
Lower Zambezi
Rise
Beira High
AFRICA
Fig. 9
Fig. 6
Fig. 7
Fig. 8
Fig. 10A
N
0
100 km
Unit SU9
0
ms (TWTT)
> 1000
Thickness
Angoche
Middle Zambezi
Shelf
Slope
Lower Zambezi
Rise
Beira High
AFRICA
Fig. 9
Fig. 6
Fig. 7
Fig. 8
Fig. 10A
N
0
100 km

Figure 12

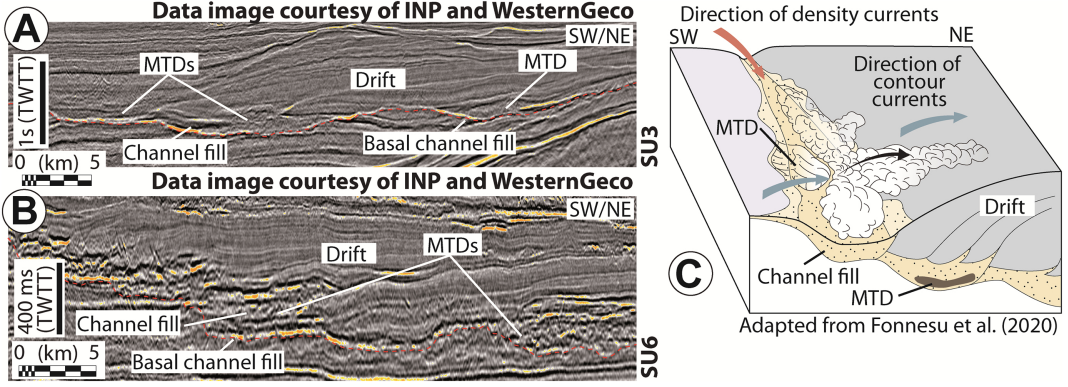
A
Data image courtesy of INP and WesternGeco
SW/NE
MTDs
Drift
MTD
1s (TWTT)
Channel fill
Basal channel fill
0 (km) 5
SU3
B
Data image courtesy of INP and WesternGeco
SW/NE
Drift
MTDs
400 ms (TWTT)
Channel fill
0 (km) 5
Basal channel fill
SU6
Direction of density currents
SW
NE
Direction of contour currents
MTD
Drift
C
Channel fill
MTD
Adapted from Fonnesu et al. (2020)

Figure 13

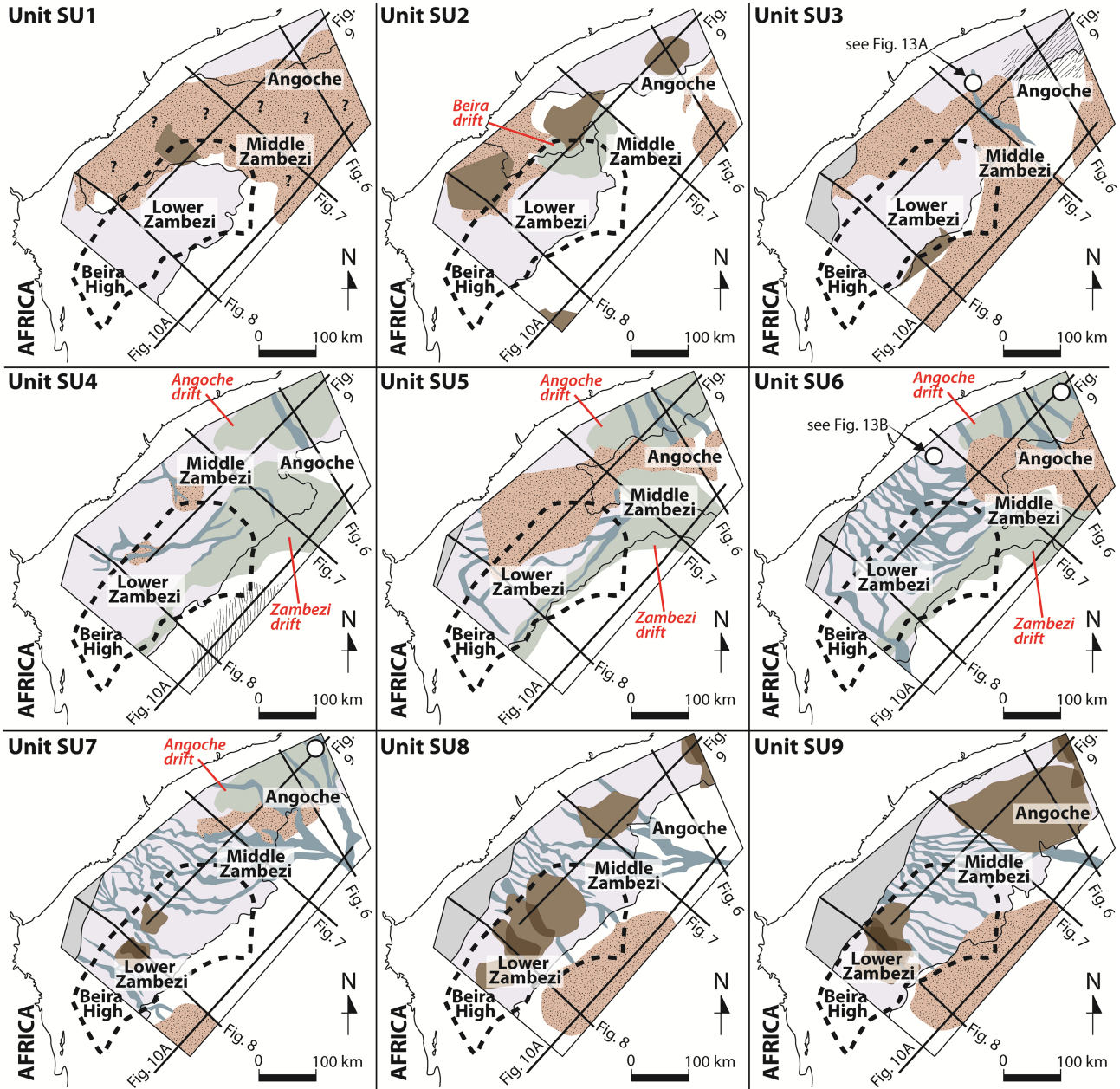
Unit SU1
Unit SU2
Unit SU3
Unit SU4
Unit SU5
Unit SU6
Unit SU7
Unit SU8
Unit SU9
Angoche
Middle Zambezi
Lower Zambezi
Beira High
Beira drift
Angoche drift
Zambezi drift
see Fig. 13A
see Fig. 13B
AFRICA
N
0
100 km
Fig. 6
Fig. 7
Fig. 8
Fig. 9
Fig. 10A
Shelf
Irregular and erosive slope
Channels
Large contourite drifts
Sedimentary lobes
Large sediment waves field
MTDs
Smooth rise
Beira High limit
Small contourite drifts

Figure 14

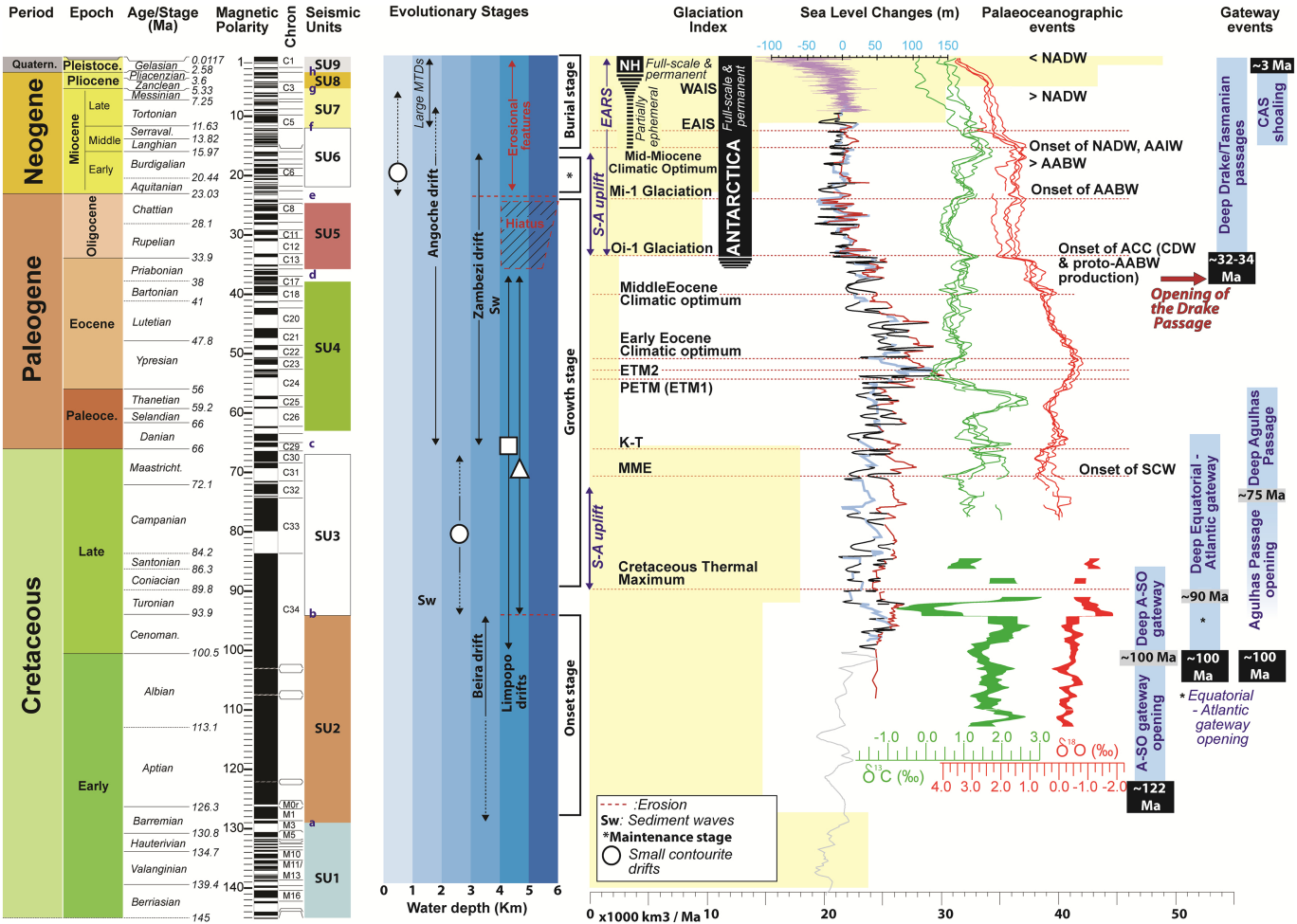
Period
Epoch
Age/Stage (Ma)
Magnetic Polarity
Chron
Seismic Units
Evolutionary Stages
Glaciation Index
Sea Level Changes (m)
Palaeoceanographic events
Gateway events
Quatern.
Pleistoc.
Pliocene
Neogene
Miocene
Late
Middle
Early
Oligocene
Paleogene
Eocene
Paleoce.
Cretaceous
Late
Early
Gelasian
Piacenzian
Zanclean
Messinian
Tortonian
Serraval.
Langhian
Burdigalian
Aquitanian
Chattian
Rupelian
Priabonian
Bartonian
Lutetian
Ypresian
Thanetian
Selandian
Danian
Maastricht.
Campanian
Santonian
Coniacian
Turonian
Cenoman.
Albian
Aptian
Barremian
Hauterivian
Valanginian
Berriasian
0.0117
2.58
3.6
5.33
7.25
11.63
13.82
15.97
20.44
23.03
28.1
33.9
38
41
47.8
56
59.2
66
66
72.1
84.2
86.3
89.8
93.9
100.5
113.1
126.3
130.8
134.7
139.4
145
SU9
SU8
SU7
SU6
SU5
SU4
SU3
SU2
SU1
Large MTDs
Angoche drift
Zambezi drift
Sw
Beira drift
Limpopo drifts
Erosional features
Hiatus
Burial stage
Growth stage
Onset stage
EARS
S-A uplift
NH
Full-scale & permanent
Partially ephemeral
WAIS
EAIS
ANTARCTICA
Mid-Miocene Climatic Optimum
Mi-1 Glaciation
Oi-1 Glaciation
MiddleEocene Climatic optimum
Early Eocene Climatic optimum
ETM2
PETM (ETM1)
K-T
MME
Cretaceous Thermal Maximum
< NADW
> NADW
Onset of NADW, AAIW > AABW
Onset of AABW
Onset of ACC (CDW & proto-AABW production)
Onset of SCW
Opening of the Drake Passage
Deep Drake/Tasmanian passages
CAS shoaling
~3 Ma
~32-34 Ma
Deep Agulhas Passage
~75 Ma
Deep Equatorial - Atlantic gateway
~90 Ma
Agulhas Passage opening
Deep A-SO gateway
~100 Ma
A-SO gateway opening
~122 Ma
* Equatorial - Atlantic gateway opening
:Erosion
Sw: Sediment waves
*Maintenance stage
Small contourite drifts
Water depth (Km)
x1000 km3 / Ma

Figure 15

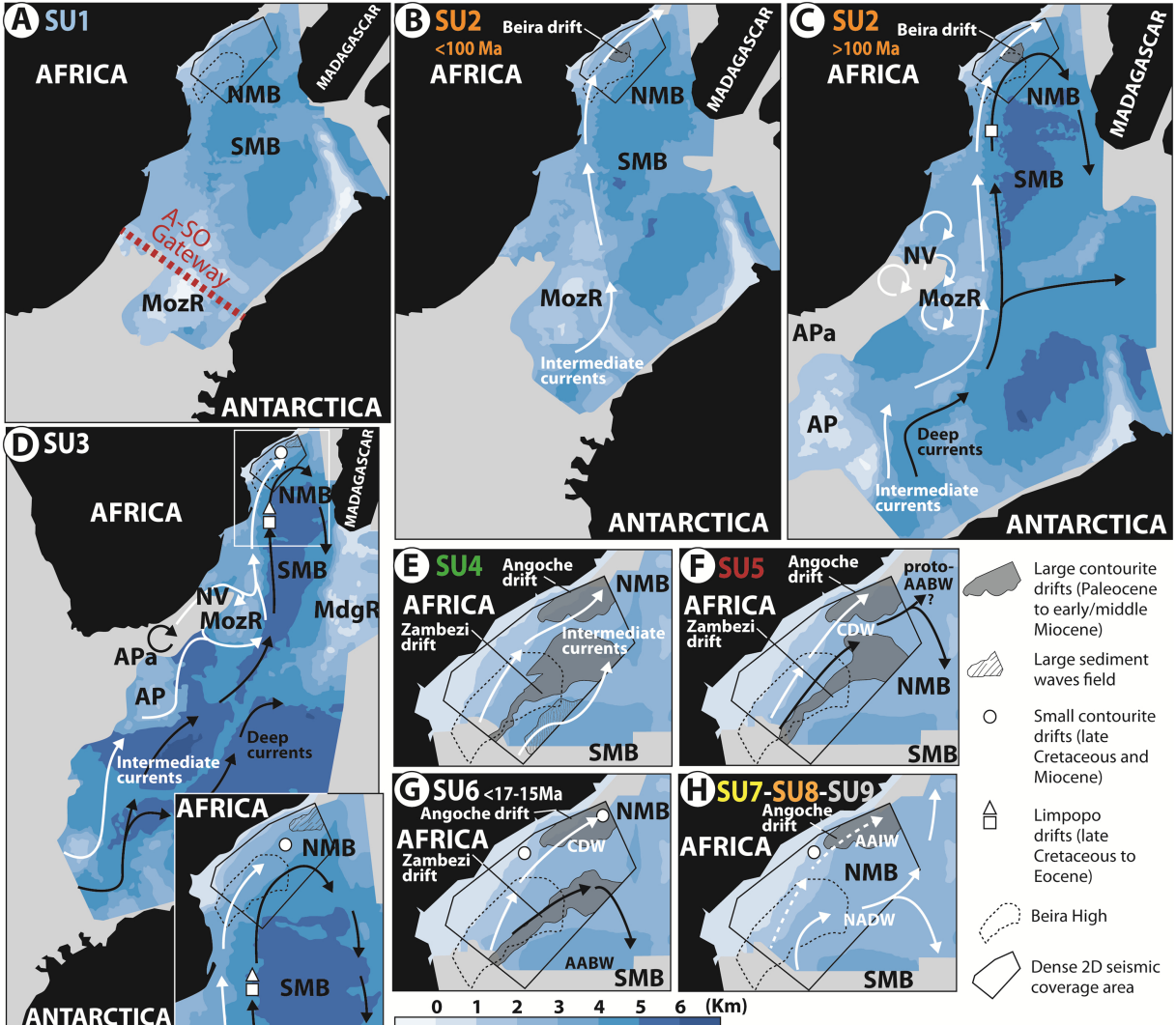
A SU1
AFRICA
MADAGASCAR
NMB
SMB
A-SO Gateway
MozR
ANTARCTICA
B SU2
<100 Ma
Beira drift
AFRICA
MADAGASCAR
NMB
SMB
MozR
Intermediate currents
ANTARCTICA
C SU2
>100 Ma
Beira drift
AFRICA
MADAGASCAR
NMB
SMB
NV
MozR
APa
AP
Deep currents
Intermediate currents
ANTARCTICA
D SU3
AFRICA
MADAGASCAR
NMB
SMB
NV
MozR
MdgR
APa
AP
Deep currents
Intermediate currents
AFRICA
NMB
SMB
ANTARCTICA
E SU4
Angoche drift
AFRICA
NMB
Zambezi drift
Intermediate currents
SMB
F SU5
Angoche drift
proto-AABW ?
AFRICA
Zambezi drift
CDW
NMB
SMB
G SU6 <17-15Ma
Angoche drift
NMB
AFRICA
Zambezi drift
CDW
AABW
SMB
H SU7-SU8-SU9
Angoche drift
AFRICA
AAIW
NMB
NADW
SMB
0 1 2 3 4 5 6 (Km)
Large contourite drifts (Paleocene to early/middle Miocene)
Large sediment waves field
Small contourite drifts (late Cretaceous and Miocene)
Limpopo drifts (late Cretaceous to Eocene)
Beira High
Dense 2D seismic coverage area

Figure 16

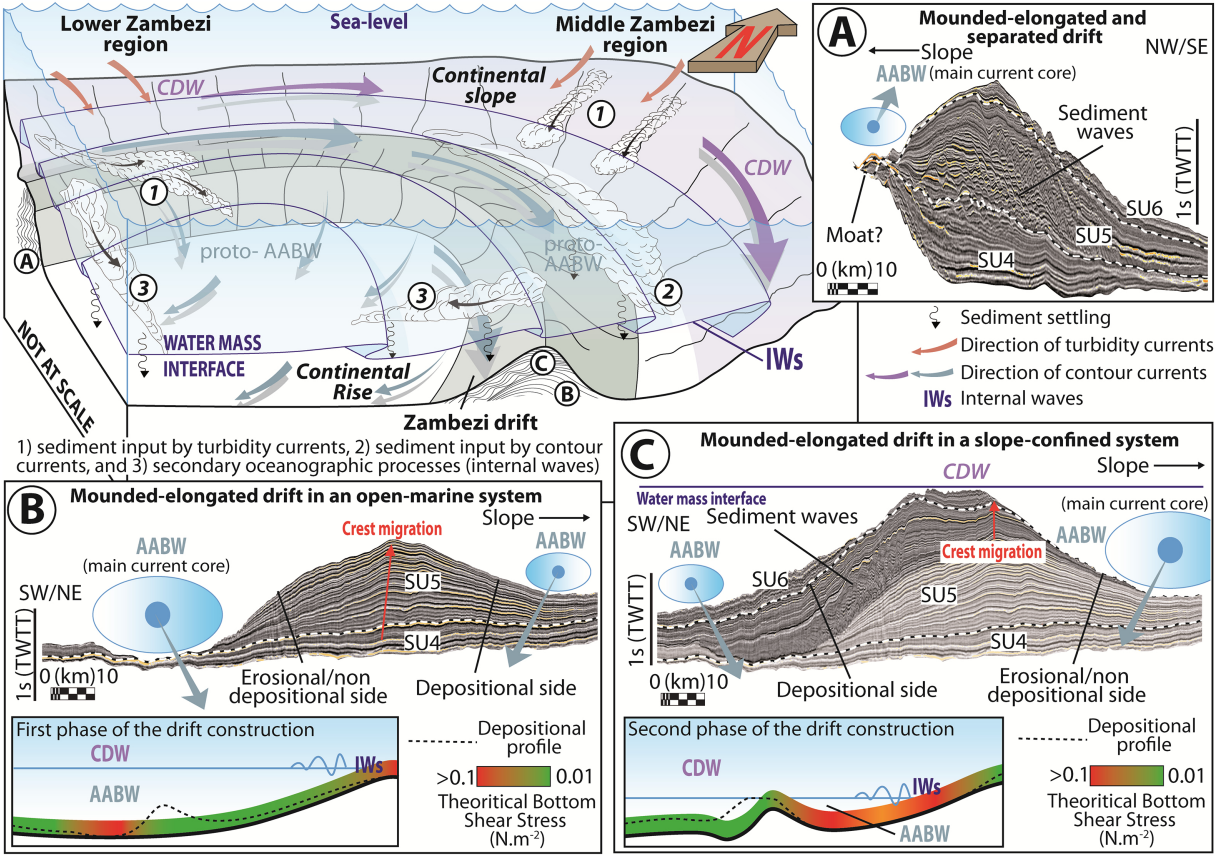
Lower Zambezi region
Sea-level
Middle Zambezi region
CDW
Continental slope
CDW
proto- AABW
proto- AABW
WATER MASS INTERFACE
Continental Rise
Zambezi drift
IWs
NOT AT SCALE
1) sediment input by turbidity currents, 2) sediment input by contour currents, and 3) secondary oceanographic processes (internal waves)
A
Mounded-elongated and separated drift
Slope
NW/SE
AABW (main current core)
Sediment waves
Moat?
SU6
SU5
SU4
1s (TWTT)
0 (km) 10
Sediment settling
Direction of turbidity currents
Direction of contour currents
IWs Internal waves
B
Mounded-elongated drift in an open-marine system
Slope
AABW
(main current core)
Crest migration
AABW
SW/NE
SU5
SU4
1s (TWTT)
0 (km) 10
Erosional/non depositional side
Depositional side
First phase of the drift construction
CDW
IWs
AABW
Depositional profile
>0.1
0.01
Theoritical Bottom Shear Stress (N.m-2)
C
Mounded-elongated drift in a slope-confined system
CDW
Slope
Water mass interface
SW/NE
Sediment waves
(main current core)
AABW
AABW
Crest migration
SU6
SU5
SU4
1s (TWTT)
0 (km) 10
Depositional side
Erosional/non depositional side
Second phase of the drift construction
CDW
IWs
AABW
Depositional profile
>0.1
0.01
Theoritical Bottom Shear Stress (N.m-2)

Figure 17

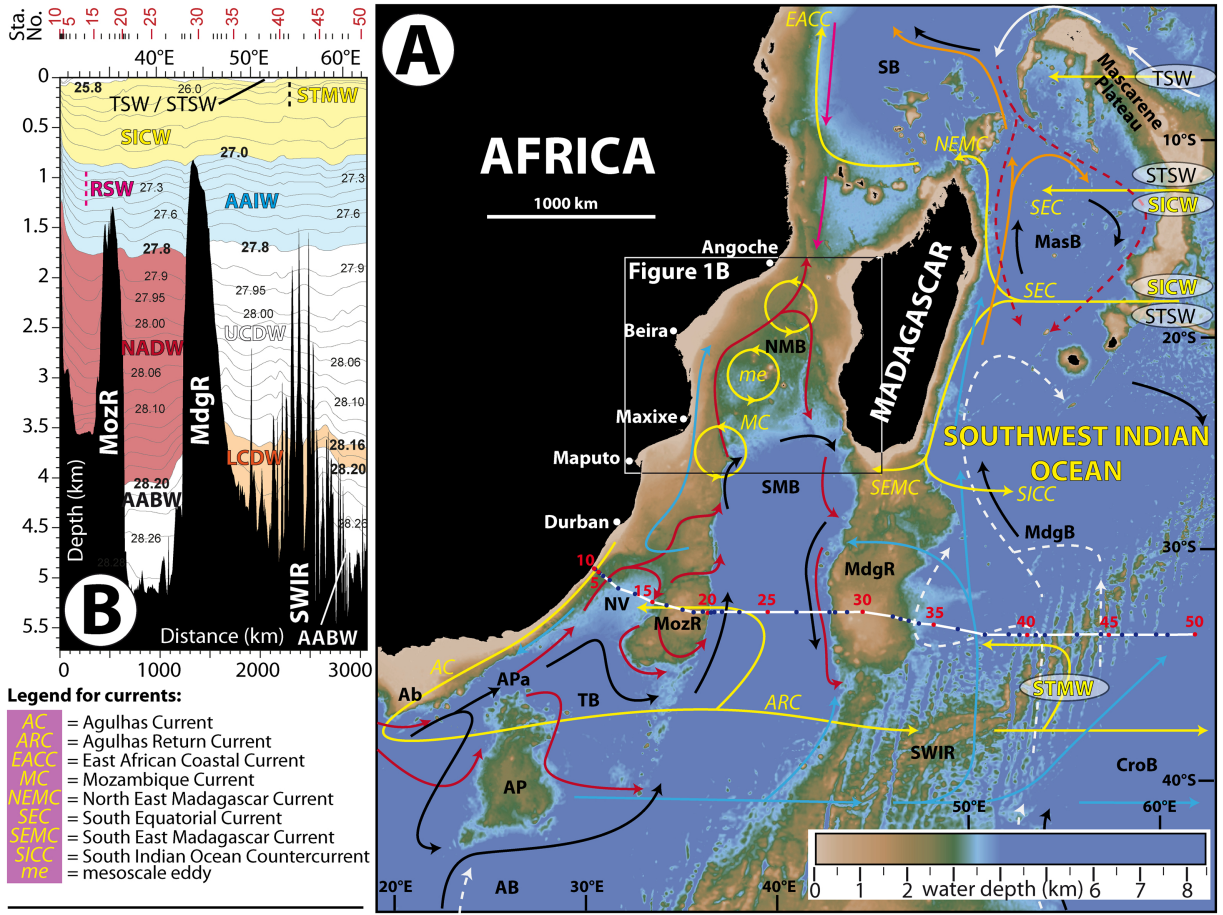
Sta. No.
40°E
50°E
60°E
TSW / STSW
STMW
SICW
RSW
AAIW
NADW
UCDW
LCDW
AABW
MozR
MdgR
SWIR
Depth (km)
Distance (km)
B
A
AFRICA
1000 km
MADAGASCAR
Figure 1B
Angoche
Beira
Maxixe
Maputo
Durban
SOUTHWEST INDIAN OCEAN
EACC
SB
NEMC
Mascarene Plateau
TSW
STSW
SICW
SEC
MasB
NMB
me
MC
SMB
SEMC
SICC
MdgB
MdgR
NV
MozR
AC
APa
Ab
TB
ARC
AP
SWIR
CroB
STMW
AB
10°S
20°S
30°S
40°S
50°E
60°E
20°E
30°E
40°E
water depth (km)
Legend for currents:
AC = Agulhas Current
ARC = Agulhas Return Current
EACC = East African Coastal Current
MC = Mozambique Current
NEMC = North East Madagascar Current
SEC = South Equatorial Current
SEMC = South East Madagascar Current
SICC = South Indian Ocean Countercurrent
me = mesoscale eddy
ANTARCTIC WATER MASSES
AAIW = Antarctic Intermediate Water
CDW = Circumpolar Deep Water
UCDW = Upper Circumpolar Deep Water
LCDW = Lower Circumpolar Deep Water
AABW = Antarctic Bottom Water
INDIAN WATER MASSES
TSW = Tropical Surface Water
STSW = Sub-Tropical Surface Water
STMW = Sub-Tropical Mode Water
SICW = South Indian Central Water
IDW = Indian Deep Water
ATLANTIC WATER MASS
NADW = North Atlantic Deep Water
RED-SEA WATER MASS
RSW = Red Sea Water

Figure 18

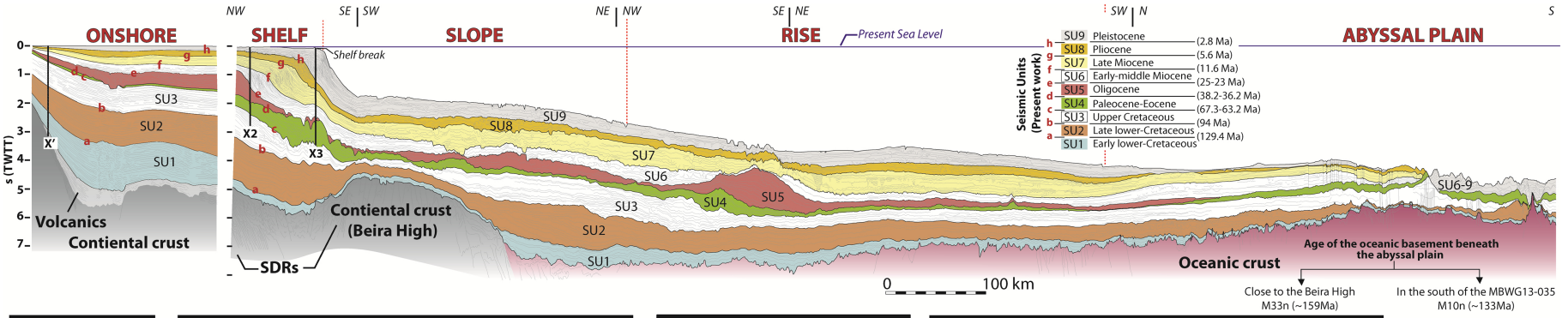
NW
SE | SW
NE | NW
SE | NE
SW | N
S
ONSHORE
SHELF
SLOPE
RISE
ABYSSAL PLAIN
Present Sea Level
Shelf break
s (TWTT)
0
1
2
3
4
5
6
7
X'
X2
X3
SU1
SU2
SU3
SU4
SU5
SU6
SU7
SU8
SU9
SU6-9
Volcanics
Contiental crust
Contiental crust
(Beira High)
SDRs
Oceanic crust
Seismic Units
(Present work)
h SU9 Pleistocene (2.8 Ma)
g SU8 Pliocene (5.6 Ma)
f SU7 Late Miocene (11.6 Ma)
e SU6 Early-middle Miocene (25-23 Ma)
d SU5 Oligocene (38.2-36.2 Ma)
c SU4 Paleocene-Eocene (67.3-63.2 Ma)
b SU3 Upper Cretaceous (94 Ma)
a SU2 Late lower-Cretaceous (129.4 Ma)
SU1 Early lower-Cretaceous
Age of the oceanic basement beneath the abyssal plain
Close to the Beira High M33n (~159Ma)
In the south of the MBWG13-035 M10n (~133Ma)
0
100 km

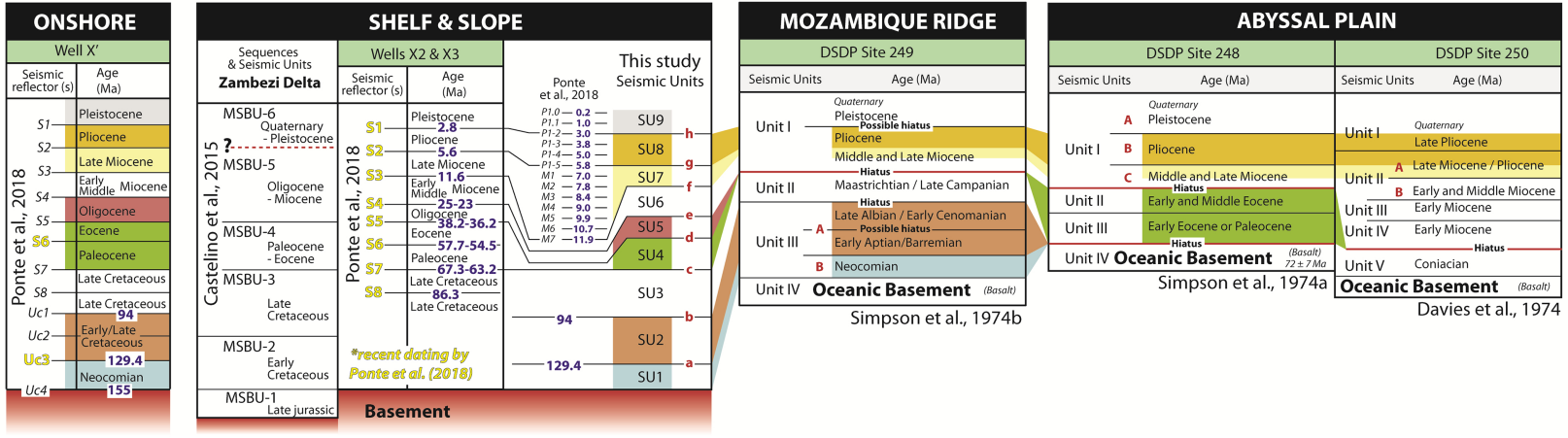
ONSHORE
Well X'
Seismic reflector (s)
Age (Ma)
Ponte et al., 2018
S1 Pleistocene
S2 Pliocene
S3 Late Miocene
S4 Early Middle Miocene
S5 Oligocene
S6 Eocene
S7 Paleocene
S8 Late Cretaceous
Late Cretaceous
Uc1 94
Uc2 Early/Late Cretaceous
Uc3 129.4
Uc4 Neocomian 155
SHELF & SLOPE
Sequences & Seismic Units
Zambezi Delta
Castelino et al., 2015
MSBU-6 Quaternary - Pleistocene
MSBU-5 Oligocene - Miocene
MSBU-4 Paleocene - Eocene
MSBU-3 Late Cretaceous
MSBU-2 Early Cretaceous
MSBU-1 Late jurassic
Wells X2 & X3
Seismic reflector (s)
Age (Ma)
Ponte et al., 2018
S1 Pleistocene 2.8
S2 Pliocene 5.6
S3 Late Miocene 11.6
S4 Early Middle Miocene 25-23
S5 Oligocene 38.2-36.2
S6 Eocene 57.7-54.5
S7 Paleocene 67.3-63.2
S8 Late Cretaceous 86.3
Late Cretaceous
*recent dating by Ponte et al. (2018)
Basement
Ponte et al., 2018
This study Seismic Units
P1.0 0.2
P1.1 1.0
P1-2 3.0
P1-3 3.8
P1-4 5.0
P1-5 5.8
M1 7.0
M2 7.8
M3 8.4
M4 9.0
M5 9.9
M6 10.7
M7 11.9
SU9 h
SU8 g
SU7 f
SU6 e
SU5 d
SU4 c
SU3
94 b
SU2
129.4 a
SU1
MOZAMBIQUE RIDGE
DSDP Site 249
Seismic Units
Age (Ma)
Unit I Quaternary Pleistocene
Possible hiatus
Pliocene
Middle and Late Miocene
Hiatus
Unit II Maastrichtian / Late Campanian
Unit III A Late Albian / Early Cenomanian
Possible hiatus
Early Aptian/Barremian
B Neocomian
Unit IV Oceanic Basement (Basalt)
Simpson et al., 1974b
ABYSSAL PLAIN
DSDP Site 248
Seismic Units
Age (Ma)
Unit I A Quaternary Pleistocene
B Pliocene
C Middle and Late Miocene
Hiatus
Unit II Early and Middle Eocene
Unit III Early Eocene or Paleocene
Hiatus
Unit IV Oceanic Basement (Basalt) 72 ± 7 Ma
Simpson et al., 1974a
DSDP Site 250
Seismic Units
Age (Ma)
Unit I Quaternary Late Pliocene
A Late Miocene / Pliocene
Unit II B Early and Middle Miocene
Unit III Early Miocene
Unit IV Early Miocene
Hiatus
Unit V Coniacian
Oceanic Basement (Basalt)
Davies et al., 1974

Figure 19

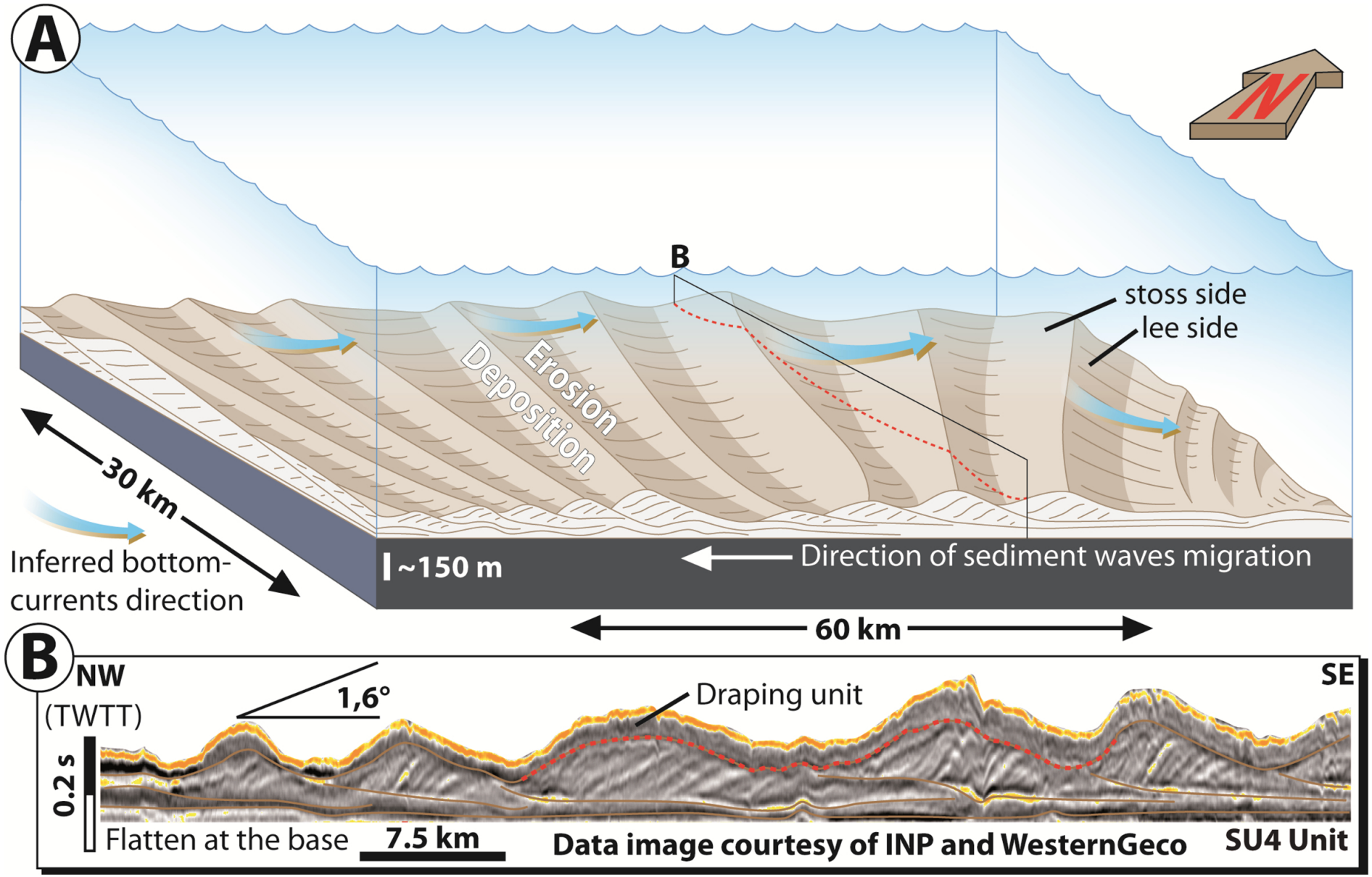
A
N
B
stoss side
lee side
Deposition
Erosion
30 km
Inferred bottom-currents direction
~150 m
Direction of sediment waves migration
60 km
B
NW
SE
(TWTT)
1,6°
Draping unit
0.2 s
Flatten at the base
7.5 km
Data image courtesy of INP and WesternGeco
SU4 Unit

Figure 20